Cell Reports

Article

Splenic marginal zone B cells restrict *Mycobacterium tuberculosis* infection by shaping the cytokine pattern and cell-mediated immunity

Graphical abstract

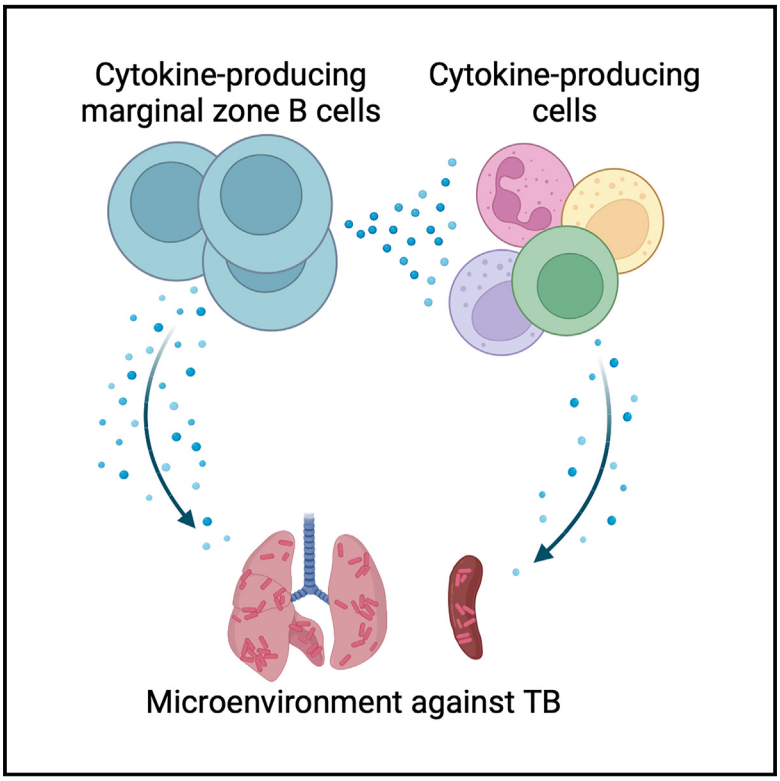

Authors

Chen-Yu Tsai, Myo Oo, Jih Hou Peh, ..., Thomas Dick, Katja Fink, Martin Gengenbacher

Correspondence

martin.gengenbacher@gmail.com

In brief

Tsai et al. show that marginal zone B cells accumulate in the lungs and spleen in response to *Mycobacterium tuberculosis* infection, exhibiting activated, memory-like phenotypes and producing multiple cytokines. Splenic marginal zone B cells restrict infection by coordinating the systemic cytokine pattern and cell-mediated immunity.

Highlights

- MZB cells accumulate in the lungs and spleen in response to Mtb infection
- MZB cells produce multiple cytokines during infection
- Splenic MZB cells restrict infection by shaping cytokine patterns
- Splenic MZB cells restrict infection by orchestrating cell-mediated immunity

Tsai et al., 2024, Cell Reports *43*, 114426
July 23, 2024
https://doi.org/10.1016/j.celrep.2024.114426

CellPress

Cell Reports

CellPress
OPEN ACCESS

Article

Splenic marginal zone B cells restrict *Mycobacterium tuberculosis* infection by shaping the cytokine pattern and cell-mediated immunity

Chen-Yu Tsai,[1] Myo Oo,[1] Jih Hou Peh,[2] Benjamin C.M. Yeo,[3] Ariel Aptekmann,[1] Bernett Lee,[4,5,6] Joe J.J. Liu,[2] Wen-Shan Tsao,[1] Thomas Dick,[1,7] Katja Fink,[4] and Martin Gengenbacher[1,7,8,*]

[1]Center for Discovery and Innovation (CDI), Hackensack Meridian Health, 111 Ideation Way, Nutley, NJ 07110, USA
[2]Biosafety Level 3 Core, Yong Loo Lin School of Medicine, National University of Singapore (NUS), Level 15, Centre for Translational Medicine (MD6), NUS, 14 Medical Drive, Singapore 117599, Singapore
[3]Infectious Diseases Translational Research Programme and Department of Medicine, Yong Loo Lin School of Medicine, National University of Singapore (NUS), Level 2, Blk MD4, 5 Science Drive 2, Singapore 117545, Singapore
[4]Singapore Immunology Network (SIgN), Agency for Science Technology and Research, Biopolis, 8A Biomedical Grove, Level 3 & 4, Immunos Building, Singapore 138648, Singapore
[5]Centre for Biomedical Informatics, Lee Kong Chian School of Medicine, Nanyang Technological University, 50 Nanyang Avenue, Singapore 639798, Singapore
[6]A*STAR Infectious Diseases Labs, Agency for Science, Technology and Research, 8A Biomedical Grove #05-13, Immunos, Singapore 138648, Singapore
[7]Hackensack Meridian School of Medicine, Nutley, NJ 07110, USA
[8]Lead contact
*Correspondence: martin.gengenbacher@gmail.com
https://doi.org/10.1016/j.celrep.2024.114426

SUMMARY

Understanding the role of B cells in tuberculosis (TB) is crucial for developing new TB vaccines. However, the changes in B cell immune landscapes during TB and their functional implications remain incompletely explored. Using high-dimensional flow cytometry to map the immune landscape in response to *Mycobacterium tuberculosis* (Mtb) infection, our results show an accumulation of marginal zone B (MZB) cells and other unconventional B cell subsets in the lungs and spleen, shaping an unconventional B cell landscape. These MZB cells exhibit activated and memory-like phenotypes, distinguishing their functional profiles from those of conventional B cells. Notably, functional studies show that MZB cells produce multiple cytokines and contribute to systemic protection against TB by shaping cytokine patterns and cell-mediated immunity. These changes in the immune landscape are reversible upon successful TB chemotherapy. Our study suggests that, beyond antibody production, targeting the regulatory function of B cells may be a valuable strategy for TB vaccine development.

INTRODUCTION

Mycobacterium tuberculosis (Mtb) is a severe public health threat worldwide, causing 1.6 million deaths per year.[1] One of the primary challenges in controlling tuberculosis (TB) is the lack of reliable vaccines. The Bacille Calmette-Guérin (BCG) vaccine, the only licensed vaccine for TB, shows varying efficacy, ranging from 0% to 80%.[2] The development of an effective alternative to BCG has been hampered by an incomplete understanding of the immune correlates for protection against TB. Over the past 4 decades, research has predominantly focused on the role of T cells in Mtb infection. CD4 T cells have been demonstrated as a major player in controlling Mtb infection.[3–6] In addition, CD8 T cells have been shown to provide protection against TB.[7–10] However, despite B cells being crucial players in combating infectious diseases, their role in TB is still not fully understood. Therefore, elucidating their role in immunity and protection in TB may provide valuable insights for developing TB vaccines.

The role of B cells in TB is complex and remains a subject of ongoing debate. Previous studies have shown that B cells can play protective[11–15] or detrimental[16] or even neutral roles[17,18] during Mtb infection. This inconsistency may result from the use of different animal models and Mtb strains across these studies. Despite the varied roles of B cells in Mtb burden, they consistently influence wide-range immune responses from mouse to non-human primate models, such as immunopathology,[11,12,16] cytokine patterns,[11,12,15] and neutrophil[12] and T cell[12,14–16] responses. Collectively, these studies highlight a significant regulatory role of B cells in diverse immune responses during TB.

B cells comprise heterogeneous subsets that display distinct functional characteristics, thereby providing a broad defense spectrum against infections. B cell subsets can be categorized

into conventional and unconventional B cells based on their functional characteristics and immunophenotypes. Conventional B cells, also termed follicular B (FoB) cells, represent the major B cell subset,[19–23] comprising around 80% of B cells.[20,21] As the critical component for adaptive immunity,[24] FoB cells react to infections by generating high-affinity antibodies.[20,24] In contrast, unconventional B cells, including marginal zone B (MZB) cells, B1 B cells, MZB cell precursors (MZPs), and age-associated B cells (ABCs), exhibit characteristics distinct from those of FoB cells.[20–23,25–27] As components of innate immunity,[21] MZB and B1 cells respond to infections more rapidly than FoB cells by primarily releasing low-affinity antibodies.[28,29] MZPs serve as precursors of MZB cells.[28,30] In addition, ABCs are found in aged mice and several infectious and autoimmune diseases.[25–27] In infectious diseases, ABCs are associated with long-term protection against several intracellular pathogens.[25,31,32]

B cells dynamically alter their subset compositions to tailor the response to TB.[33–35] Studies have shown that the frequency of MZB cells increases in the blood of active TB patients,[36] and the frequencies of atypical B cells with the ABC phenotype increase in the blood of both active and latent TB patients.[33,36] In mice, B1 B cells emerge in the lungs during Mtb infection.[35] Notably, the successful treatment of TB has been found to reverse the alterations in B cell subset compositions.[33] These observations suggest that B cells change their immune landscape in response to the varying status of Mtb infection.

Despite the documented changes in B cell subsets in TB, the detailed dynamics of these alterations and their functional implications remain incompletely understood. To comprehensively investigate the detailed immune landscape of B cells, we used high-dimensional flow cytometry to analyze B cell subsets in infected organs of mouse models. The utilization of high-dimensional flow cytometry allowed for comprehensive analysis of B cell subsets, offering a complete immune landscape. Subsequently, we depleted the specific B cell subset in mouse models to examine their functional implications on Mtb infection. Our results revealed that, in response to Mtb infection in the lungs and spleen, B cells shifted their immune landscape toward MZB cells, contributing to systemic protection by shaping cytokine patterns and cell-mediated immunity. This suggests that, beyond their role in antibody production, B cells can leverage regulatory functions in cytokine production to protect against Mtb infection. This discovery opens a new avenue in TB vaccine development, suggesting that targeting B cells for their regulatory functions could be a promising new strategy.

RESULTS

Unconventional B cells increase in the lung and spleen in response to Mtb infection

To understand the changes in the immune landscape of B cells throughout Mtb infection, we mapped the landscape in the lungs and spleen of Mtb-infected mice using high-dimensional flow cytometry. The experimental scheme is illustrated in Figure 1A (top). Briefly, mice were infected with 100–200 bacilli of Mtb H37Rv through an aerosol. Mice infected with the same amount of γ-irradiated Mtb H37Rv served as mock controls to mimic exposure without causing infection. Uninfected mice served as baseline controls. Lungs and spleen were harvested at 4, 8, and 12 weeks post-infection. Single-cell suspensions of the lungs and spleen were analyzed by flow cytometry. In line with the previous publication,[37] in the lungs, Mtb load rose to a peak at the acute phase (0–4 weeks), slightly declined, and subsequently stabilized at the chronic phase (4–12 weeks); in the spleen, Mtb load constantly increased throughout the chronic phase (Figure 1A, bottom).

For B cell immunophenotyping, mature B cells ($B220^{+}CD93^{-}$) were gated into four subsets: MZB ($CD1d^{hi}CD23^{lo}$), FoB ($CD1d^{mi}CD23^{hi}$), MZP ($CD1d^{hi}CD23^{hi}$), and ABC ($CD1d^{mi}CD23^{lo}$). The gating strategy is adopted from previous studies[21–23,30,38] and depicted in Figures 1B and S1A.

Our results revealed an expansion of unconventional B cell subsets, changing the immune landscape of B cells in infected organs. MZB cells were detected in the lungs of infected mice (representative plots in Figure 1C). This observation is notable because mouse MZB cells are typically found in the spleen.[21] With rare exceptions, phenotypically similar cells were observed in extrasplenic locations under specific conditions,[22,39–43] such as in the lymph nodes in aged mice[22] or in autoimmune diseases, like type 1 diabetes[39] and autoimmune arthritis.[22] The frequencies of pulmonary and splenic MZB cells progressively increased throughout the infection compared to mock controls (Figure 1D). In contrast, the frequencies of FoB cells, the conventional B cell subset, diminished in the lungs and spleen of infected mice (Figure 1E, representative plots in Figure 1C). MZPs were also detected in the infected lungs (representative plots in Figure 1C), and their frequencies in the lungs and spleen increased during infection (Figure 1F). Moreover, the frequency of pulmonary ABCs increased in response to the infection (Figure 1G, representative plots in Figure 1C). All B cell subsets increased their absolute counts in the lungs and spleen in response to infection (Figures S1B–S1E). MZB cells had the highest fold increase among all B cell subsets, implying their significant role in immune responses in TB (Figure 1H). The results showed that pulmonary MZB cells were localized inside the B cell follicles, a hallmark of TB pathology in the lungs,[44,45] and splenic MZB cells resided in the marginal zone of the spleen (Figures S1G and S1H). In summary, B cells changed their immune landscape in response to Mtb infection by expanding MZB cells and other unconventional B cell subsets.

Pulmonary and splenic MZB cells share similar immunophenotypes and RNA signatures but differ from conventional B cells

Given the uncommon presence of MZB cells, MZPs, and ABCs in the lungs, we further characterized their identities by analyzing the expression spectra of additional surface markers. Given the high expression of CD9 on MZB cells[46] and MZPs,[30] we used CD9 expression to characterize the identities of pulmonary MZB cells and MZPs. Our results showed that pulmonary MZB cells and MZPs had higher frequencies of $CD9^{+}$ cells than FoB cells, patterns consistent with their splenic counterparts (Figures 2A and 2D). In addition, given the prominent CD21 expression on MZB cells[21,47] and MZPs,[30] and the low expression on ABCs, we used CD21 as another distinguishing marker. Notably, pulmonary MZB cells did not express a higher level of

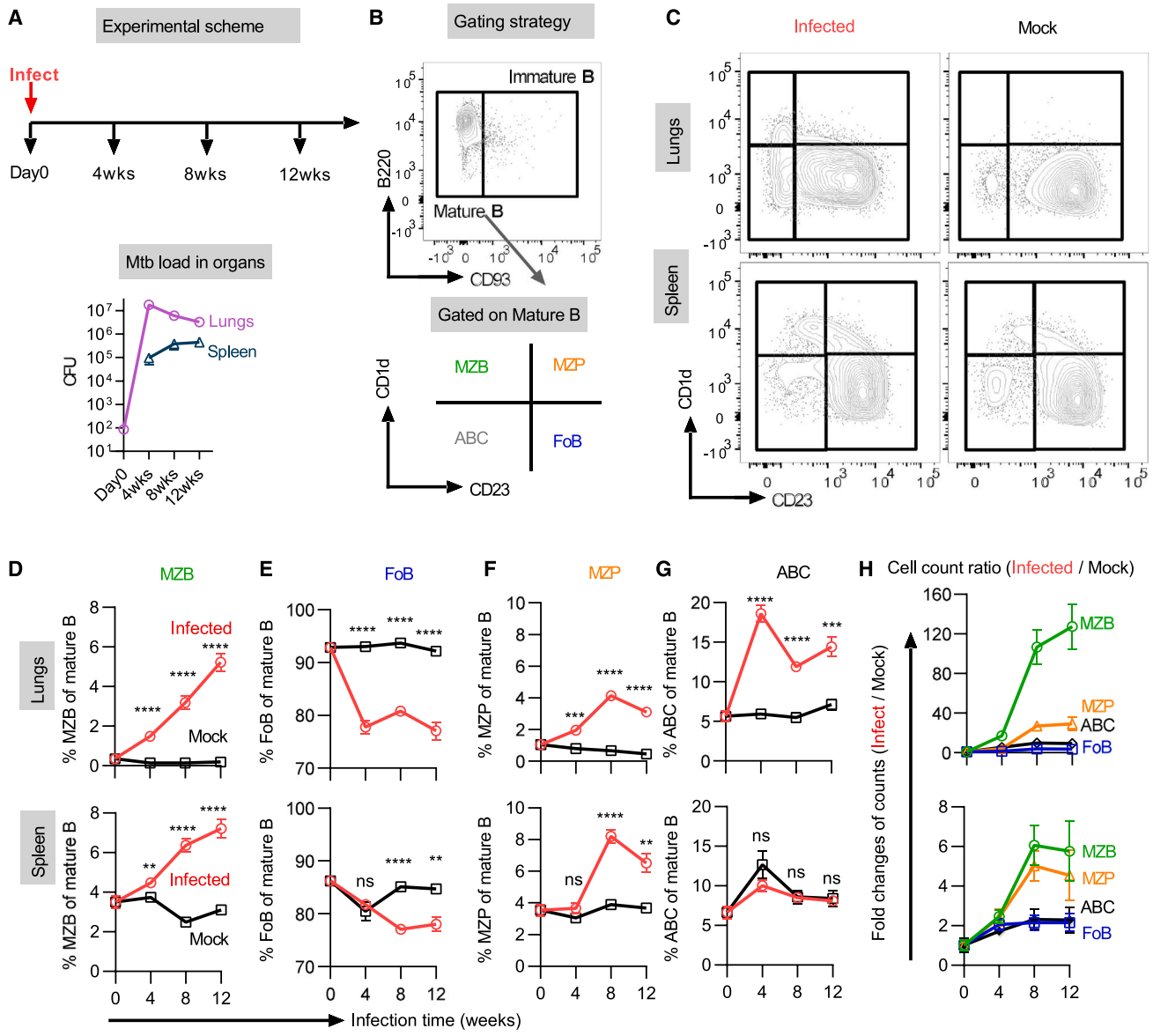

Figure 1. MZB cells increase in the lung and spleen in response to Mtb infection

Mice were infected with 100–200 CFU of Mtb via aerosol infection. Mice exposed to the same amount of γ-irradiated Mtb served as mock-infected controls. Mice were sacrificed at 4, 8, and 12 weeks post-infection. Uninfected mice served as baseline controls (0 weeks).

(A) Schematic design of the experiment and bacterial burden in the lungs and spleen. Mean ± SEM, $n = 4$. Error bars are omitted if shorter than the symbols.

(B and C) Single-cell suspensions of the lungs and spleen were analyzed by flow cytometry. (B) Gating strategy for B cell subsets. The complete gating strategy is shown in Figure S1A. (C) Representative plots of B cell subsets.

(D–G) Frequencies of each B cell subset of mature B cells in the lungs and spleen. (D) MZB, (E) FoB, (F) MZP, and (G) ABC. Mean ± SEM, $n = 4$–6. Error bars are omitted if shorter than the symbols. Unpaired Student's t test was used to determine the statistical differences between Mtb-infected and mock-infected groups. $^{**}p < 0.01$, $^{***}p < 0.001$, $^{****}p < 0.0001$; ns, not significant.

(H) Ratio of cell counts for each B cell subset. The ratio was determined by dividing the cell counts in the Mtb-infected group by those in the mock-infected group. Mean ± SEM, $n = 6$. Error bars are omitted if shorter than the symbols.

The results shown are representative of three independent experiments.

CD21 than FoB cells (Figures 2B and 2D), a characteristic aligning with the expression spectra of nodal MZB cells found outside the spleen.[22] MZP cells expressed a high level of CD21, mirroring the pattern observed in splenic MZPs. In contrast, ABCs had the lowest CD21 expression and displayed CD11c expression (Figures 2B and S1F), a pattern consistent with ABCs found in other models.[25,26] In addition, given the expression of CD43 on B1 B cells or memory B cells,[21,48] we added CD43 to characterize B cell subsets. Our results showed that, like their splenic counterparts, pulmonary MZB cells, MZPs, and ABCs displayed

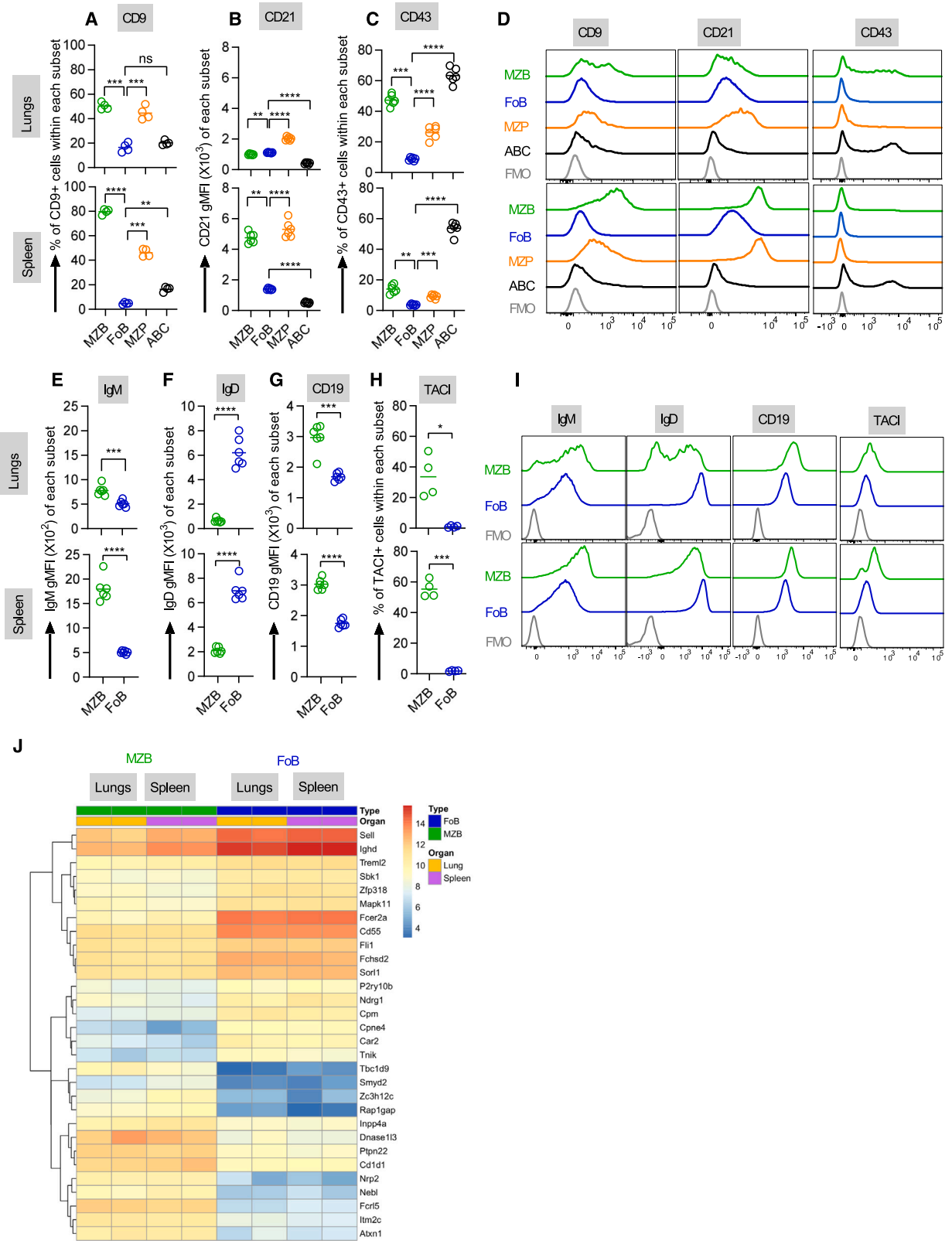

(legend on next page)

higher frequencies of CD43$^+$ cells than FoB cells, implying these subsets shared the characteristics of memory B or B1 cells. Comparison between infected and mock-infected mice showed that infection led to a decrease in CD9$^+$ cell frequencies, CD21 expression in MZB cells and MZPs, and a reduction in CD43$^+$ cell frequencies in ABCs (Figures S2A–S2C). Despite these changes, the fundamental expression patterns of these markers remained consistent across both groups. Our findings demonstrated that unconventional B -cell subsets in the lungs had expression spectra similar to those of their splenic counterparts and differed from conventional B cells.

Considering the notable presence of MZB cells in the infected lungs, we explored additional defining features of these cells. Given that splenic MZB cells are known to express higher levels of IgM, CD19, and CD267 (TACI) and lower levels of IgD,[21,49] we examined the expression spectra of these markers on pulmonary MZB cells. As anticipated, our results showed that pulmonary MZB cells had expression spectra similar to those of splenic MZB cells with higher IgM and lower IgD expression, as well as higher CD19 expression and TACI$^+$ cell frequency, compared to FoB cells (Figures 2E–2I). Comparison between infected and mock-infected mice revealed that Mtb infection affected the frequencies or expression levels of specific markers but did not alter the fundamental expression patterns of these markers on MZB and FoB cells (Figures S2D–S2G). The findings further confirmed a high degree of similarity between the protein-level characteristics of pulmonary and splenic MZB cells.

We further compared the RNA signature between pulmonary and splenic MZB cells. Single-cell suspensions were generated from the infected lungs and spleen at 12 weeks post-infection. MZB and FoB cells were sorted (Figure S2J) and subjected to RNA sequencing (RNA-seq). The results showed that pulmonary MZB cells had RNA signatures similar to those of splenic MZB cells (Figure 2J). As expected, pulmonary and splenic MZB cells displayed different RNA signatures compared with their FoB counterparts (Figure 2J). In summary, pulmonary MZB cells shared protein and RNA characteristics with splenic MZB cells but differed from conventional B cells.

MZB cells display activated phenotypes and serve as memory-like B cells during Mtb infection

To understand the functional phenotypes of MZB cells in Mtb infection, we first examined whether MZB cells exhibited the activated phenotype. This phenotype was determined by the upregulation of CD86, CD80, and CD69, surface markers that are characteristically increased in activated B cells.[50,51] These markers play critical roles in the immune functions of B cells: CD86 and CD80 play as immune regulatory ligands to regulate functions of T cells through interaction with CD28 family receptors.[52,53] CD69 contributes to the retention of lymphocytes in lymphoid organs.[54] Our results showed that the frequencies of CD86$^+$ cells and levels of CD86 expression increased in all B cell subsets in response to infection (Figures 3A and S4A and representative plots in S3A). Remarkably, MZB cells displayed the highest frequency of CD86$^+$ cells among all subsets (Figure 3C). Although not all B cell subsets increased CD80 expression following infection (Figures S4C and representative plots in S3C), MZB cells still presented the highest frequencies of CD80$^+$ cells among all subsets (Figure 3C). The notable presence of CD86$^+$ and CD80$^+$ cells in MZB cells suggests their superior potential to regulate T cell functions by providing ligands for CD28 family receptors compared to other subsets. For CD69 expression, all B cell subsets increased frequencies of CD69$^+$ cells and the levels of CD69 expression in response to infection (Figures 3B and S4B and representative plots in S3B), particularly in the lungs. Pulmonary MZB cells contained a higher frequency of CD69$^+$ cells than their FoB counterparts (Figure 3C), possibly contributing to the maintenance of MZB cells within infected lungs compared to conventional B cells. In conclusion, our results revealed that MZB cells display activated phenotypes in response to infection, potentially empowering them with a greater capacity to regulate immune functions within infected tissues than conventional B cells.

Subsequently, we investigated whether MZB cells served as memory B cells during infection, because nodal MZB cells have been shown to display the memory-like phenotype in aged mice.[22] B cells expressing CD80, CD273, and CD73 were identified as memory-like B cells[55–57] (the gating strategy and representative plots are shown in Figures S3D–S3G). Our results showed that the pulmonary MZB cells exhibited the highest frequency of memory-like B cells among all subsets (Figure 3D). Similarly, splenic MZB cells displayed a higher frequency of memory-like B cells than FoB cells and MZPs (Figure 3D). Although previous studies have shown that memory B cells can display either the FoB or the MZB phenotype,[58,59] our observation highlighted that, in response to Mtb infection,

Figure 2. Pulmonary MZB cells have similar immunophenotypes and RNA signatures compared to splenic MZB cells

Single-cell suspensions were prepared from the lungs and spleen at 8 weeks post-infection and analyzed by flow cytometry.

(A–C) Expression spectra of CD9, CD21, and CD43 on MZB cells, FoB cells, MZPs, and ABCs. B cell subsets were gated according to Figure S1A. The CD9- and CD43-expressing cells were identified by fluorescence minus one (FMO) controls. (A) Frequencies of CD9$^+$ cells, (B) gMFI (geometric mean fluorescence intensity) of CD21, and (C) frequencies of CD43$^+$ cells. Horizontal lines represent the mean, $n = 4–6$; one-way repeated-measures ANOVA with Bonferroni's *post hoc* test was used to determine the statistical differences between subsets. $^{**}p < 0.01$, $^{***}p < 0.001$, $^{****}p < 0.0001$; ns, not significant.

(D) Representative histograms of CD9, CD21, and CD43 expression.

(E–H) Expression spectra of surface markers on MZB and FoB cells. B cell subsets were gated according to Figure S2I. (E) gMFI of IgM, (F) gMFI of IgD, (G) frequencies of CD19$^+$ cells, and (H) frequencies of TACI$^+$ cells. Horizontal lines represent the mean, $n = 4–6$; paired Student's t test was used to determine the statistical differences between subsets. $^{*}p < 0.05$, $^{***}p < 0.001$, $^{****}p < 0.0001$.

(I) Representative histograms of IgM, IgD, CD19, and TACI expression. The results shown are representative of two or three independent experiments (A–H).

(J) Heatmap represents the top 30 most significant differential gene expressions between MZB and FoB cells, ranked by adjusted *p* value, illustrating cell-type-specific transcriptional signatures. The adjusted *p* value was corrected using the Benjamini-Hochberg method at a false discovery rate (FDR) < 0.05. MZB and FoB cells were purified from the lungs and spleen at 12 weeks post-infection (Figure S2J) and underwent RNA-seq. Each group included pooled samples from 12 mice. Results from two independent experiments are shown.

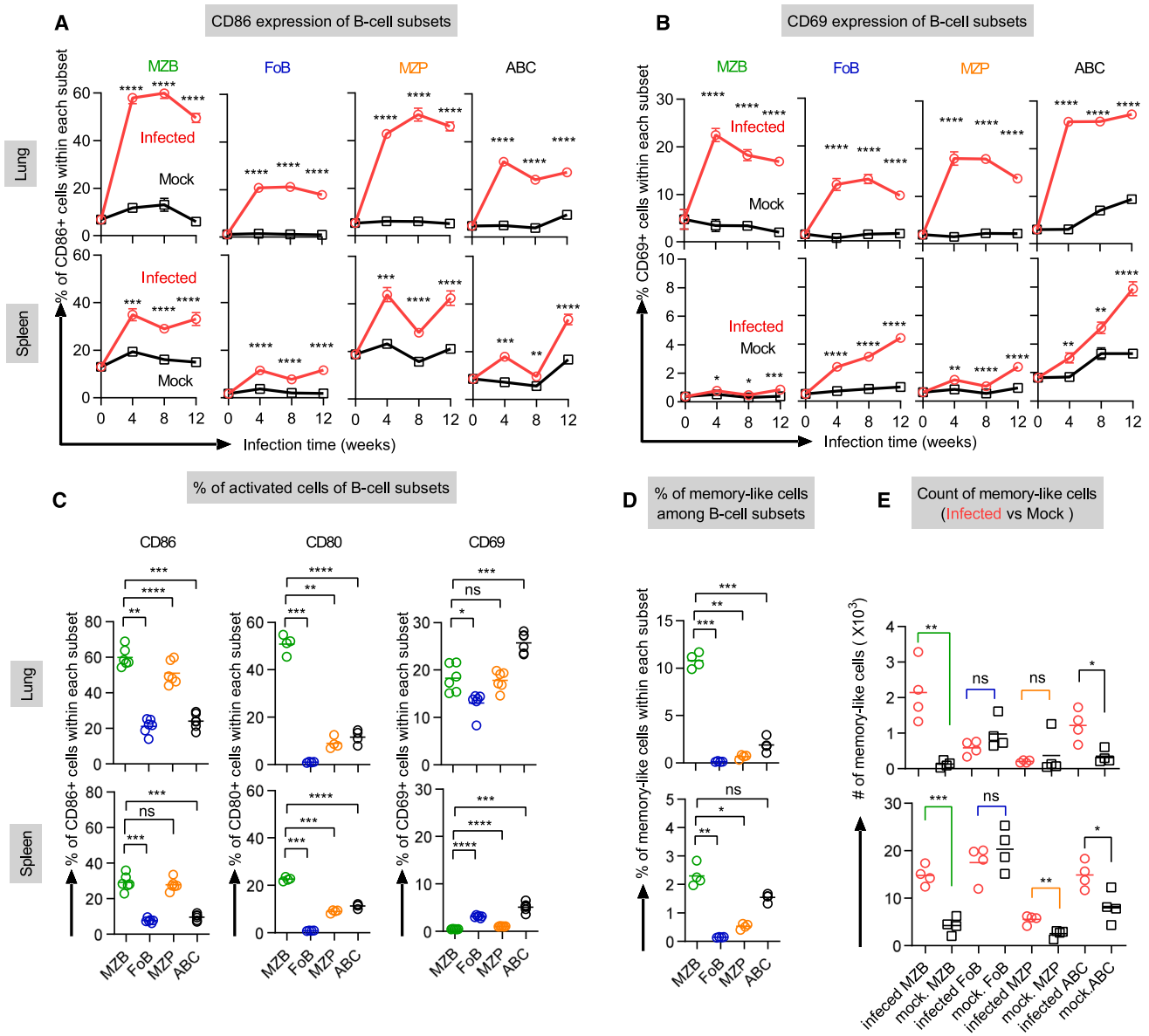

Figure 3. MZB cells display activated phenotypes and serve as memory-like B cells during Mtb infection

Infected mice and corresponding mock controls were sacrificed at 4, 8, and 12 weeks post-infection, with uninfected mice serving as baseline controls (0 weeks). Single-cell suspensions of the lungs and spleen were analyzed by flow cytometry. The B cell subsets were gated according to Figure S1A.

(A and B) Expression patterns of CD86 and CD69 on B cell subsets. (A) Frequencies of $CD86^+$ cells and (B) frequencies of $CD69^+$ cells. Mean ± SEM, $n = 4–6$. Error bars are omitted if shorter than the symbols. Unpaired Student's t test was used to determine the statistical differences between Mtb-infected and mock controls. $^*p < 0.05$, $^{**}p < 0.01$, $^{***}p < 0.001$, $^{****}p < 0.0001$.

(C and D) Activated and memory-like phenotypes of B cell subsets in infected mice at 8 weeks post-infection. (C) Frequencies of $CD86^+$, $CD80^+$, and $CD69^+$ cells and (D) frequencies of memory-like B cells ($CD80^+CD273^+CD73^+$). Horizontal lines represent the mean, $n = 4–6$; one-way repeated-measures ANOVA with Bonferroni's *post hoc* test was used to determine the statistical differences between subsets. $^*p < 0.05$, $^{**}p < 0.01$, $^{***}p < 0.001$, $^{****}p < 0.0001$; ns, not significant.

(E) Absolute counts of memory-like B cells within B cell subsets in infected and mock-infected mice at 8 weeks post-infection. Horizontal lines represent the mean, $n = 4$. Unpaired Student's t test was used to determine the statistical differences between Mtb-infected and mock controls. $^*p < 0.05$, $^{**}p < 0.01$, $^{***}p < 0.001$; ns, not significant.

The results shown are representative of three independent experiments.

memory-like B cells preferentially increased in absolute count within the MZB subset rather than the FoB subset (Figure 3E). In addition, memory-like B cells increased in absolute counts within ABC and MZP subsets, but the most pronounced elevation was observed within the MZB subsets. In summary, MZB cells serve as a reservoir for accumulating memory-like cells in response to infection, setting them apart functionally from conventional B cells in TB.

MZB cells contribute to systemic TB control by shifting cytokine patterns to create an anti-TB environment

To investigate the functional role of MZB cells during Mtb infection, we depleted MZB cells in infected mice using anti-CD11a and anti-CD49d antibodies, as described in the literature.[60–63] The experimental design is illustrated in Figure 4A. Briefly, mice received the blocking antibodies intraperitoneally 1 day before Mtb inoculation and subsequently received the antibodies weekly throughout the infection. Mice that received isotype control antibodies served as controls. As expected, the blocking antibodies significantly reduced the frequencies and counts of splenic MZB cells, particularly in the first 4 weeks (Figures 4B and 4C). However, these antibodies failed to deplete pulmonary MZB cells (Figures 4B and 4C), despite prominent expression of CD11a and CD49d on these cells (Figures S4D and S4E), suggesting that the depletion of pulmonary MZB cells may involve additional factors other than CD11a and CD49d. The depletion of splenic MZB cells resulted in an increased Mtb burden in the spleen at 4–8 weeks post-infection compared to controls (Figures 4D and S6A), indicating their contribution to local protection. Importantly, this depletion also led to an increased Mtb burden in the lungs at 8 weeks post-infection (Figure 4D), underscoring the systemic protective role of splenic MZB cells.

Given that B cells are known to secrete cytokines to regulate systemic immune responses,[64] we investigated whether the alterations in the cytokine pattern could be responsible for the elevated Mtb load following the depletion of MZB cells. We measured the levels of cytokines in plasma in MZB-depleted mice and controls. Remarkably, the depletion of splenic MZB cells resulted in a shift of the cytokine pattern in circulation that was associated with promoting TB progression (Figures 4E and 4F). Particularly, at later time points, the depletion significantly decreased the levels of TNF-α, CXCL1, CCL5, IL-2, GM-CSF, and IL-13 (Figure 4E). Among these, TNF-α,[65,66] CCL5,[67] IL-2,[68,69] GM-CSF,[70–72] and CXCL1[73,74] have previously been associated with restricting Mtb growth. In contrast, the depletion of splenic MZB cells increased the levels of IL-10, IL-1α, IL-4, IL-12p70, and CCL4 (Figure 4F). IL-10[75–77] and IL-4[78–80] have been reported to promote Mtb growth. Therefore, the alteration in cytokine pattern correlated with the increased Mtb burden, suggesting that MZB cells achieved systemic protection against TB by shaping the cytokine pattern.

MZB cells produce multiple cytokines against TB

Because the depletion of splenic MZB cells altered the systemic cytokine pattern, we examined whether MZB cells would directly produce cytokines against infection. To mimic the exposure to Mtb components, the single-cell suspensions of the lungs and spleen from infected mice were stimulated with Mtb lysate *ex vivo*, and cytokine production was subsequently measured using intracellular staining. Uninfected mice served as controls to assess whether naive MZB cells also responded to Mtb components by producing cytokines without prior exposure. Our results showed that both pulmonary and splenic MZB cells displayed higher frequencies of multiple cytokine-producing B cells than FoB cells in infected mice (Figures 5A–5E). In particular, MZB cells had the highest frequencies of TNF-α^+, CXCL1$^+$, and GM-CSF$^+$ cells among all subsets (Figures 5A, 5B, and 5E; representative plots in Figure S5A). Naive MZB cells from uninfected mice exhibited a similar cytokine response to Mtb lysate (Figures 5F–5J and S5B–S5K), suggesting their inherent capacity for multiple-cytokine production. This indicated that MZB cells employed multiple-cytokine production as an innate immune defense against TB. Therefore, our results indicated that MZB cells exhibit a robust ability to directly produce multiple cytokines against TB, distinguishing their function from conventional B cells.

We further analyzed whether multiple-cytokine-producing B cells specifically accumulated within the MZB subset in response to the infection. The results showed that multiple-cytokine-producing B cells consistently increased their absolute counts in the MZB subset in infected mice compared to uninfected controls (Figures 5K–5O). In contrast, multiple-cytokine-producing B cells did not consistently increase their counts in other B cell subsets (Figures 5K–5O), although MZPs and ABCs also could produce cytokines against Mtb lysate (Figures 5A–5E). Upon analysis of the frequencies of cytokine-producing cells within the MZB subset, results showed that Mtb infection generally did not increase these frequencies (Figures S5B–S5F). Therefore, the quantitative expansion in MZB cells increased the pool for accumulating multiple-cytokine-producing B cells against Mtb infection.

MZB cells orchestrate humoral and cell-mediated immunity to mediate protection against TB

Given that B cells use antibody production as the central mechanism for systematically controlling infections,[24] we examined whether the change in antibody levels could account for the elevated Mtb load following the depletion of MZB cells. We measured the levels of purified protein derivative (PPD)-reactive IgM, IgG, and IgA in the plasma of MZB-depleted mice and controls. Our results showed that the depletion of splenic MZB cells temporarily decreased the PPD-reactive IgM level but had no impact on IgG and IgA levels (Figure 6A). This observation was paralleled by a decrease in the frequency of splenic IgM$^+$ plasma cells early in infection (Figures S6B), showing splenic MZB cells as precursors to IgM$^+$ plasma cells. Therefore, splenic MZB cells may provide protection against TB through IgM-mediated mechanisms.

Splenic MZB cells have been reported to regulate systemic T cell responses against brain tumors[81]; therefore, we examined whether changes in T cell responses could account for the increased Mtb burden following the depletion of splenic MZB cells. Our results showed that the depletion of splenic MZB cells temporarily delayed the accumulation of CD8 T cell counts without affecting CD4 T cell counts in the lungs (Figures 6B and 6C), leading to alterations in CD4 and CD8 T cell frequencies at early time points (Figures S6E and S6F). In the spleen, the depletion of splenic MZB cells did not significantly affect the counts of CD4 and CD8 T cells (Figures 6B and 6C); however, it caused increased CD4 T and decreased CD8 T frequencies (Figures S6E and S6F). In addition, this depletion led to increased counts of $\gamma\delta$ T cells at 4 weeks post-infection in the lungs and spleen (Figure 6D). Therefore, MZB cells may also contribute to the protection against TB by regulating T cell responses.

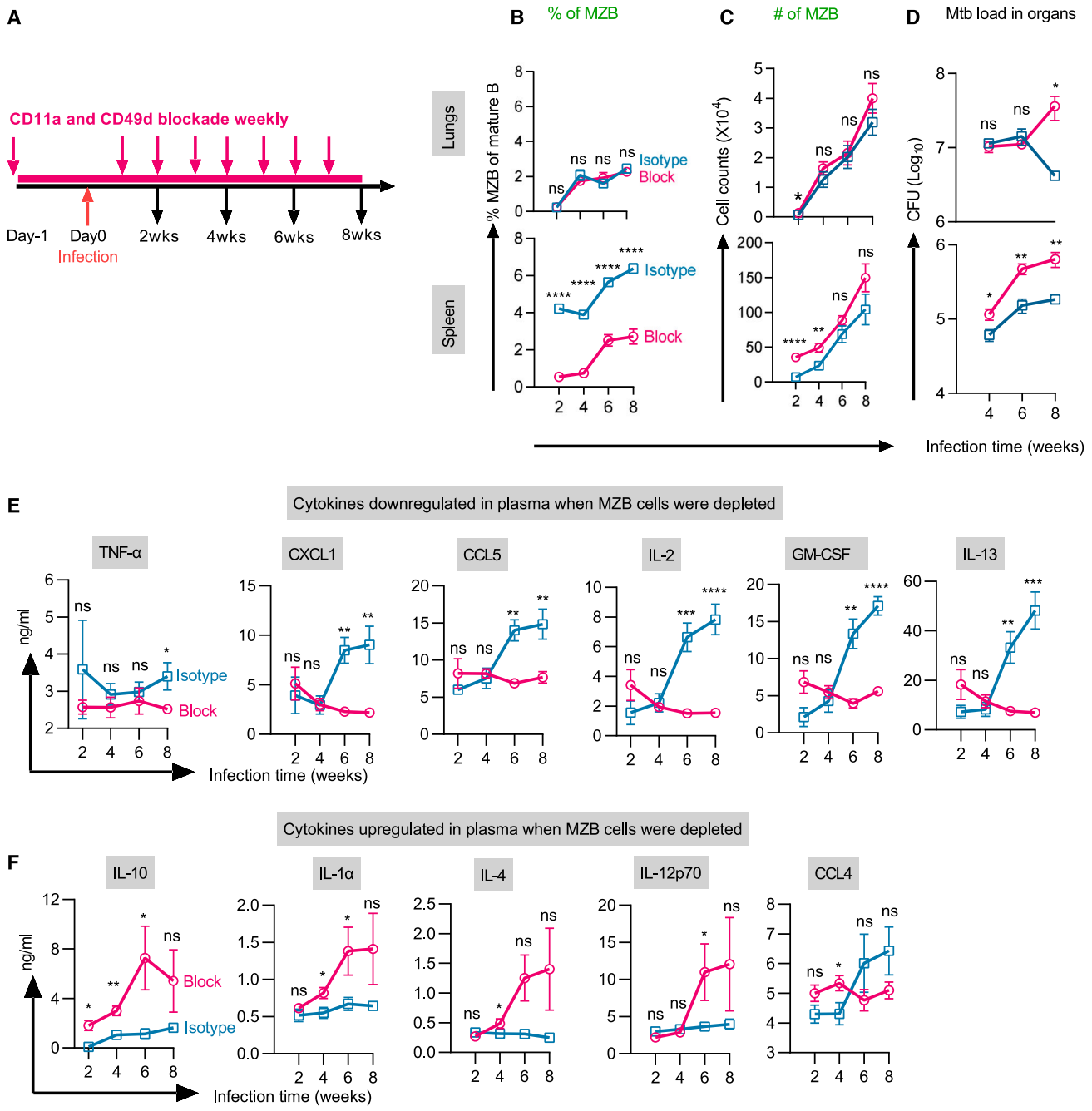

Figure 4. MZB cells contribute to systemic tuberculosis control by shifting cytokine patterns to favor an anti-tuberculosis environment

Mice received anti-CD11a and anti-CD49d antibodies to deplete MZB cells 1 day prior to infection. Subsequently, mice were infected with aerosolized Mtb and consistently received the same dose of depletion antibodies every week until sacrifice. Control mice underwent the same experimental procedure but were given corresponding isotype control antibodies. Mice were sacrificed at 2, 4, 6, and 8 weeks post-infection.

(A) Schematic design of experiment.

(B and C) MZB cells were gated according to Figure S1A. (B) Frequencies of MZB cells. (C) Counts of MZB cells, $n = 8$.

(D) Bacterial burden in the lungs and spleen, $n = 7–8$.

(E and F) Cytokine patterns in plasma. The levels of cytokines and chemokines were measured by multiplex analysis. (E) Downregulated cytokines in MZB-depleted mice and (F) upregulated cytokines in MZB-depleted mice, $n = 3–8$. Mean ± SEM. Error bars are omitted if shorter than the symbols. Unpaired Student's t test was used to determine the statistical differences between MZB-depleted and control mice. $^{*}p < 0.05$, $^{**}p < 0.01$, $^{***}p < 0.001$, $^{****}p < 0.001$; ns, not significant. The results shown are representative of two independent experiments.

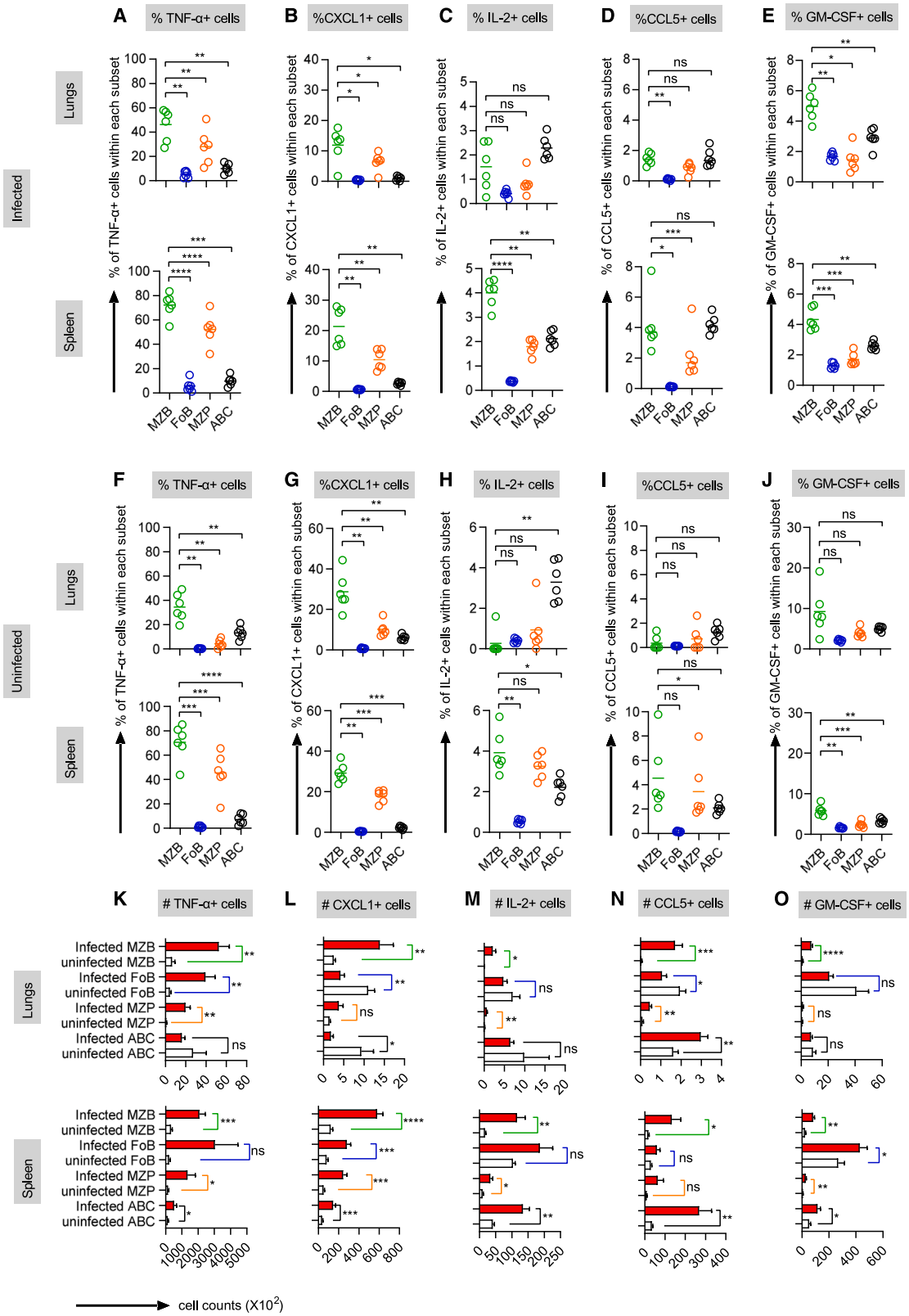

(legend on next page)

To investigate whether the changes in innate-like immune cells correlated to the elevated Mtb load following the depletion of MZB cells, we also examined the responses of natural killer (NK) cells, CD1d-restricted invariant natural killer T (iNKT) cells, and granulocytes in MZB-depleted mice and their controls. The results showed that the depletion of splenic MZB cells decreased the NK cell counts in both the lungs and the spleen (Figure 6E); conversely, the depletion increased iNKT cell counts only in the lungs (Figure 6F) and granulocyte counts only in the spleen (Figure 6G). In addition, the depletion increased cell subsets that were enriched with macrophages, dendritic cells (DCs), and monocytes in the spleen at 4 weeks post-infection (Figure 6H). Therefore, MZB cells potentially contribute to protection against Mtb infection by orchestrating the response of innate-like immune cells.

Reduction of Mtb reverses the accumulation and activation of MZB cells

To examine whether accumulation and activation of MZB cells would persist after the resolution of infection, we analyzed the immune landscape of B cells in infected mice after treatment by antimycobacterial chemotherapy. Briefly, mice were infected with Mtb for 8 weeks to develop immunophenotypic changes in B cells and subsequently received chemotherapy for another 6 weeks (Figure 7A). The infected mice without treatment served as controls. As expected, the chemotherapy reduced the Mtb burden to 120 CFU in the lungs and an undetectable level in the spleen at the end of treatment (Figure 7B). With the reduction of Mtb burden, the frequencies and counts of MZB cells, MZPs, and ABCs decreased in the lungs and spleen of the mice on chemotherapy compared to untreated mice (Figures 7C and S7A). At the end of chemotherapy in the spleen, eradication of Mtb abolished the accumulation of MZB cells, and the immune landscape of B cells returned to background levels as in uninfected mice (Figure S7B). Notably, the persistence of low Mtb burden in the lungs prevented the frequency of MZB cells from returning to the background level (Figure S7B), highlighting that MZB cells accumulated in response even to the small amount of Mtb. In summary, the accumulation of MZB cells and the immune landscape formed by unconventional B cells gradually diminished following the clearance of Mtb infection. To investigate whether the clearance of Mtb infection would also reverse the activation of MZB cells, we measured the expression of CD86 and CD69 on MZB cells. With the reduction of Mtb burden, MZB cells and other B cell subsets decreased the frequencies of $CD86^+$ cells in both the lungs and the spleen of mice on chemotherapy compared to untreated mice (Figure 7D). After Mtb eradication in the spleen at the end of chemotherapy, MZB cells and other B cell subsets decreased their frequencies of $CD86^+$ cells to background levels (Figure S7C). Remarkably, the persistence of low Mtb burden in the lungs prevented the frequencies of $CD86^+$ cells in MZB and other unconventional B cells from decreasing to background levels. These observations highlighted that MZB cells and other unconventional B cells displayed greater sensitivity in CD86 expression to low levels of Mtb burden compared to conventional B cells.

Similarly, after Mtb eradication in the spleen, MZB cells and other B cell subsets decreased the frequency of $CD69^+$ cells, returning to the background (Figures 7E and S7D). In contrast, in response to residual Mtb burden, none of the B cell subsets decreased the frequency of $CD69^+$ cells in the lungs (Figures 7E and S7D). Especially, MZB cells maintained the highest frequency of $CD69^+$ cells (Figure 7E), which could facilitate their tissue residency. In summary, B cells reverted their activation and immune landscape to background levels after Mtb clearance. On the other hand, our results also highlight that B cells displayed sensitivity to low levels of Mtb burden by continuing to express activation markers and maintain an unconventional landscape.

DISCUSSION

In response to Mtb infection, MZB cells expanded in the lungs and spleen (Figure 1), creating an unconventional immune landscape of B cells that was associated with the control of infection (Figure 4D). MZB cells exhibit diverse roles in different infectious diseases, including protection[61,82] and exacerbation.[62,83] In *Staphylococcus aureus* and *Borrelia burgdorferi* infections, MZB cells are crucial in participating in the early immune response[28,29,82,84,85] and providing protection.[61,82] Importantly, our results showed that MZB cells continuously expanded throughout Mtb infection (Figures 1D–1G and S1B–S1E), suggesting their engagement not only during the early stage but also in the chronic phase of TB. MZB cells displayed an activated and memory-like phenotype, indicating their functional distinction from conventional B cells (Figure 3). The expansion of MZB cells increased the pool of multiple-cytokine-producing B cells (Figure 5), thereby shaping the systemic cytokine patterns (Figures 4E and 4F). Therefore, the accumulation of MZB cells not only changed the composition of B cells throughout the infection but altered the effector functions of B cells.

Figure 5. MZB cells produce multiple cytokines against TB

Mice were sacrificed at 11 weeks post-infection. Single-cell suspensions of lungs and spleen were restimulated by Mtb lysates for 6 h. Uninfected mice served as uninfected controls. Cytokine production was assessed by intracellular staining and analyzed via flow cytometry. B cell subsets were gated according to Figure S1A.

(A–E) Frequencies of cytokine/chemokine-producing cells in B cell subsets from infected mice. (A) TNF-α, (B) CXCL1, (C) IL-2, (D) CCL-5, and (E) GM-CSF.

(F–J) Frequencies of cytokine/chemokine-producing cells in B cell subsets from uninfected mice. (F) TNF-α, (G) CXCL1, (H) IL-2, (I) CCL-5, and (J) GM-CSF. Horizontal lines represent the mean, $n = 6$; one-way repeated-measures ANOVA with Bonferroni's *post hoc* test was used to determine the statistical differences between subsets. $^*p < 0.05$, $^{**}p < 0.01$, $^{***}p < 0.001$, $^{****}p < 0.0001$; ns, not significant.

(K–O) Counts of cytokine/chemokine-producing cells in B cell subsets. (K) TNF-α, (L) CXCL1, (M) IL-2, (N) CCL-5, and (O) GM-CSF. Mean ± SEM, $n = 6$; unpaired Student's t test was used to determine the statistical differences between Mtb-infected and uninfected controls. $^*p < 0.05$, $^{**}p < 0.01$, $^{***}p < 0.001$, $^{****}p < 0.001$; ns, not significant.

The results shown are representative of two independent experiments.

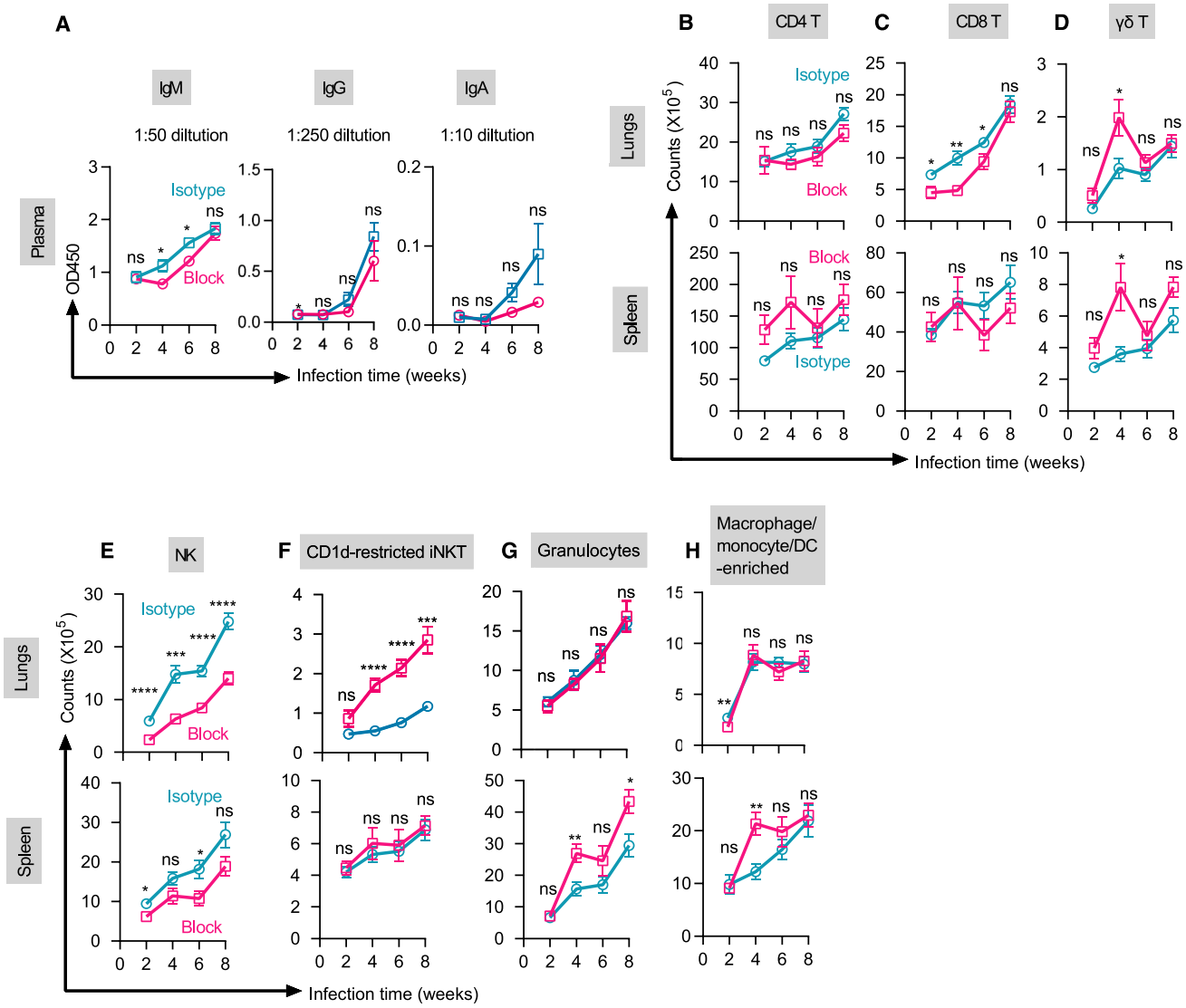

Figure 6. MZB cells orchestrate humoral and cell-mediated immunity to mediate protection against TB

MZB-depleted mice and their control mice were sacrificed at 2, 4, 6, and 8 weeks post-infection. The experimental designs are illustrated in Figure 4A.

(A) The levels of anti-PPD IgM, IgG, and IgA in the plasma samples were measured using ELISA at specified dilution factors.

(B–H) The dynamics of various immune cells in the lungs and spleen. Absolute counts of (B) CD4 T cells, (C) CD8 T cells, (D) γδ T cells, (E) NK cells, (F) CD1d-restricted iNKT cells, and (G) granulocytes. The gating strategy is depicted in Figure S6D. (H) Cell subsets that were enriched with macrophages, dendritic cells, and monocytes. The gating strategy is depicted in Figure S6C.

$n = 8$. Mean ± SEM. Error bars are omitted if shorter than the symbols. Unpaired Student's t test was used to determine the statistical differences between MZB-depleted and control mice. *$p < 0.05$, **$p < 0.01$, ***$p < 0.001$, ****$p < 0.001$; ns, not significant. The results shown are representative of two independent experiments.

Pulmonary and splenic MZB cells exhibited similar immunophenotypes and RNA signatures but differed from conventional B cells (Figure 2). These results highlight that, in response to lung infection, pulmonary MZB cells might perform functions analogous to those of splenic MZB cells, which differ from those of conventional B cells. Although MZB cells typically reside in the spleen of healthy mice,[29,49] they have been observed outside the spleen during disease progression or aging.[22,39–43] Consistent with these observations, our results confirmed the presence of B cells exhibiting the MZB phenotype and RNA signature outside the spleen during Mtb infection. However, the origins of these pulmonary MZB cells remain uncertain. We only detected a low frequency of MZB cells in the blood of infected mice (Figure S2H), suggesting that pulmonary MZB cells are unlikely to disseminate from the spleen via the bloodstream. This is further supported by our MZB depletion experiments, which did not affect the accumulation of MZB cells in the lung. More likely, pulmonary MZB cells might be derived from local FoB cells, and B cell follicles in the infected lungs could provide a suitable environment for this B cell differentiation (Figure S1G). Supporting

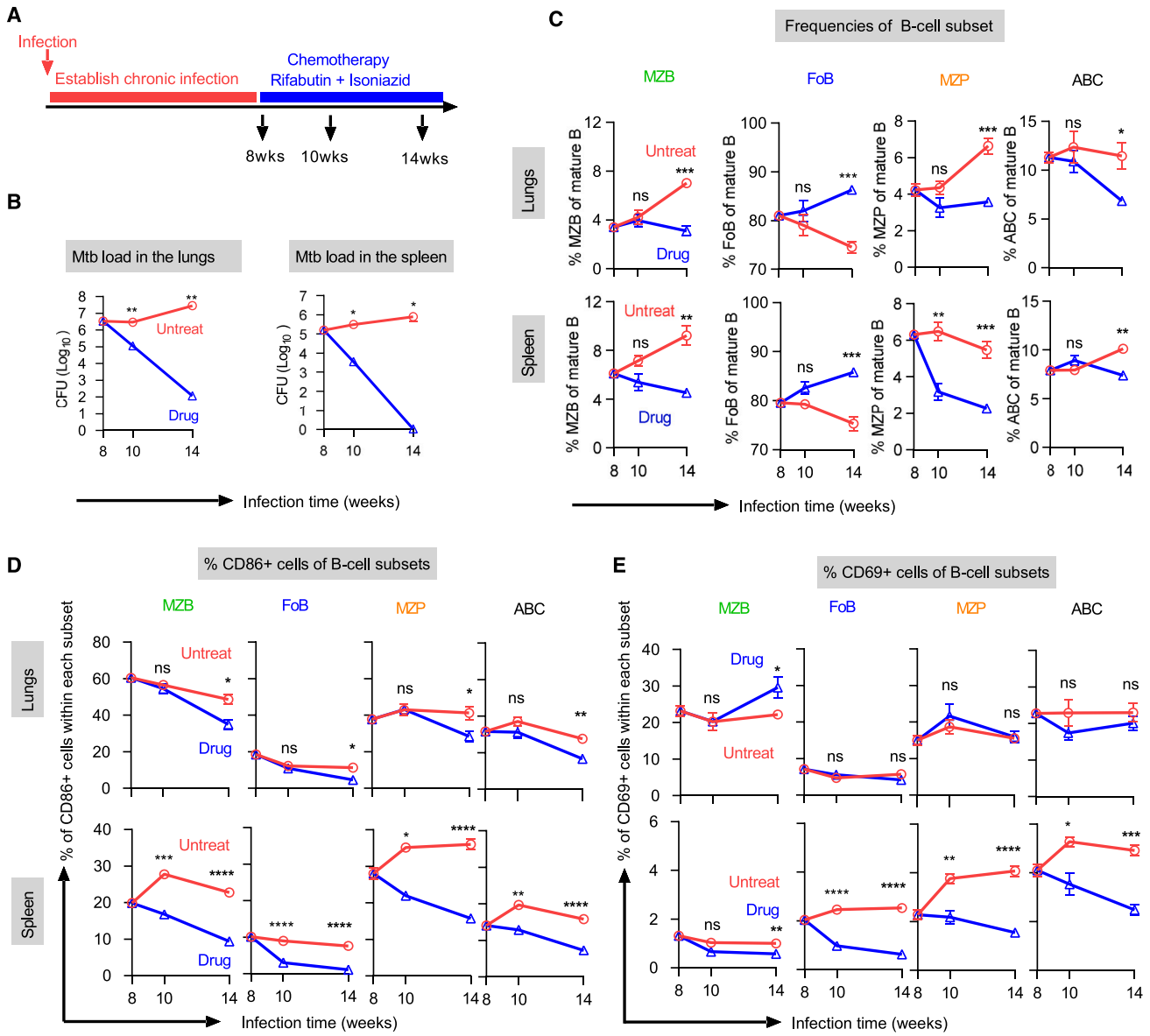

Figure 7. The clearance of Mtb infection reverses the accumulation and activation of MZB cells

Mice were infected with Mtb for 8 weeks and subsequently received chemotherapy for an additional 6 weeks. Infected mice without chemotherapy served as controls. Mice were sacrificed at 8, 10, and 14 weeks post-infection.

(A) Schematic design of the experiment.

(B) Bacterial burden in the lungs and spleen.

(C) Frequencies of B cell subsets. The subsets were gated according to Figure S1A.

(D) Frequencies of $CD86^+$ cells on B cell subsets.

(E) Frequencies of $CD69^+$ cells on B cell subsets. Mean ± SEM, $n = 4$. Error bars are omitted if shorter than the symbols. Unpaired Student's t test was used to determine the statistical differences between mice with or without chemotherapy. $^*p < 0.05$, $^{**}p < 0.01$, $^{***}p < 0.001$, $^{****}p < 0.001$; ns, not significant.

The results shown are representative of two independent experiments.

this hypothesis, FoB cells have been shown to differentiate into MZPs and subsequently into MZB cells under appropriate stimulation.[28,30,47,86] Therefore, in response to Mtb infection, pulmonary FoB cells might acquire the MZB phenotype at both protein and RNA levels to adopt the functions of splenic MZB cells. In summary, our results demonstrated the adaptability of B cells to display unconventional features in response to Mtb infection.

During Mtb infection, MZB cells displayed a distinct functional profile compared to conventional B cells, exhibiting an activated and memory-like phenotype (Figure 3). Compared to conventional B cells, MZB cells expressed higher levels of CD86 and CD80 (Figures S4A and S4B), potentially empowering them to regulate T and NK cells through interactions with CD28 family receptors,[52,53,87] a crucial mechanism in controlling TB.[88,89] The

CD86^{hi} and CD80^{hi} phenotype may contribute to their regulatory functions in the dynamics of T and NK cells within infected tissues (Figure 6). Although MZB cells are typically categorized as innate-like cells,[21] our results showed that memory-like B cells mainly accumulated in the MZB subset during infection (Figures 3D and 3E), underscoring the potential memory function of MZB cells in TB. Furthermore, with the abundant expression of CD69 on pulmonary MZB cells (Figure 3C), they potentially functioned as lung-resident memory B cells, contributing to long-term protection against Mtb infection. To support this hypothesis, a recent study shows that B cells with the CD69$^+$CD80$^+$PDL2$^+$CD73$^+$ phenotype act as lung-resident memory B cells, thereby providing protection against pneumococcal pneumonia.[90] Collectively, in response to Mtb infection, MZB cells fulfill different roles in regulating T cells and in memory functions compared to conventional B cells.

MZB cells protected against TB by shaping the cytokine pattern to foster an anti-TB environment, thereby exhibiting an unorthodox regulatory function distinct from conventional B cells. The depletion of splenic MZB cells resulted in an increased Mtb burden and the cytokine pattern that promoted TB progression (Figure 4), suggesting that MZB cells employed their regulatory abilities to restrict infection. Compared to conventional B cells, MZB cells were proficient at producing multiple cytokines (Figures 5A–5E), which are associated with protection against TB.[65,67,70,71,74,91–94] Importantly, polyfunctional CD4 T cells, co-expressing IFN-γ, TNF-α, and IL-2, play an essential role in controlling TB. Mirroring these characteristics of polyfunctional T cells, MZB cells produced both TNF-α and IL-2 (Figures 5A and 5C), essential cytokines in TB protection.[65,91,92] In addition, MZB cells produced CXCL1, CCL5, and GM-CSF (Figures 5B–5E), which could synergize with TNF-α and IL-2 to enhance TB protection. At the early stage of infection, MZB cells could provide multiple cytokines to serve as an innate defense mechanism (Figures 5F–5J), even before the onset of adaptive immunity, like polyfunctional T cells.[95] With the progression of the infection, multiple-cytokine-producing MZB cells continued to expand (Figures 5K–5O), maintaining an anti-TB environment throughout the infection. Beyond directly secreting cytokines against TB, MZB cells could utilize capacities for multiple cytokine production and co-stimulatory ligand expression (Figure 3) to regulate the dynamics of other cytokine-producing cells (Figure 6), thereby collaboratively shaping the systemic cytokine pattern to facilitate TB protection. Building on previous studies that reveal regulatory roles of B cells in immune responses to TB,[11,12,14,16,96] we further establish that MZB cells play a key role among B cells in executing the regulatory function, thereby providing protection against TB. In conclusion, our results indicate that B cells skew their immune landscape toward MZB cells to execute regulatory functions against TB, emphasizing the importance of antibody-independent mechanisms of B cells for controlling infectious diseases, a previously neglected mechanism.

Splenic MZB cells regulate cell-mediated immunity against TB in the lungs and spleen. The depletion of these cells altered the dynamics of pulmonary CD8 T and iNKT cells during infection (Figures 6C and 6F), highlighting their distal regulatory abilities. The IgM$^+$CD80$^+$CD86$^+$ phenotype (Figures 2E and 3C) potentially enabled splenic MZB cells to capture bacteria and cross-prime naive CD8 T cells within the spleen, regulating their activity in the lungs, similar to observations on the infection of *Listeria monocytogenes*.[97] In addition, splenic MZB cells may also regulate the activities of pulmonary iNKT cells (Figure 6F) through CD1d-mediated lipid antigen presentation.[98] In the spleen, the depletion of splenic MZB cells increased the frequency of CD4 T cells and counts of granulocytes and cell populations enriched with macrophages, dendritic cells, and monocytes (Figures 6G, 6H, and S6E). This suggested that splenic MZB cells may finely regulate local cell-mediated immunity to prevent excess immune responses that could exacerbate TB.[99,100] Moreover, splenic MZB cells also systemically regulated the NK and $\gamma\delta$ T cells (Figures 6D and 6E). Given that T cells, NK cells, iNKT cells, granulocytes, macrophages, dendritic cells, and monocytes can produce diverse cytokines,[101,102] MZB cells may shape the systematic cytokine pattern by regulating these cytokine-producing cells. However, because the blockade of CD11a and CD49d may also inadvertently impact these immune cells, the observed changes in cell-mediated immunity might not be solely attributed to the depletion of splenic MZB cells. In summary, MZB cells utilized their regulatory abilities to orchestrate cell-mediated immunity against TB.

Splenic MZB cells may use IgM to regulate cell-mediated immunity and cytokine patterns against TB. Splenic MZB cells differentiated into IgM$^+$ plasma cells, contributing to the systemic PPD-reactive IgM level during infection (Figures 6A and S6B). Although the role of IgM in TB is not clear in mouse models, IgM exhibited a protective role in the non-human primate model, possibly by modulating other immune components in whole blood, including various immune cells.[103] Therefore, MZB cells could utilize IgM to regulate immune cells by engaging Fc receptors. For example, the Fcμ receptor, an IgM receptor, regulates the functions of monocytes,[104] macrophages,[104] granulocytes,[104] T cells,[105] and systemic cytokine patterns[104] and contributes to protection against various infections such as *Listeria monocytogenes*,[104] *Citrobacter rodentium*,[106] lymphocytic choriomeningitis virus,[107] and influenza virus.[105] Therefore, although the direct antimicrobial effects of IgM on Mtb are not fully understood,[108] MZB cells may regulate cell-mediated immunity and cytokine patterns against TB through IgM-mediated mechanisms.

In response to Mtb infection, MZPs and ABCs accumulated, contributing to an immune landscape functionally distinct from that shaped by conventional B cells. For MZPs, our results revealed that MZPs expanded following infection in the lungs and spleen (Figures 1F and 1H). Typically, B cells with an MZP phenotype are observed outside of the spleen only in autoimmune diseases.[40,41] Pulmonary MZPs detected in infected lungs displayed characteristics similar to those of their splenic counterparts (Figures 2A–2D). Like MZB cells, MZPs exhibited an activated phenotype and produced multiple cytokines (Figures 3A–3C, 5A–5E, and S5B–S5F), suggesting a role beyond simply serving as precursors to MZB cells. Given their pronounced expression of CD80, CD86, and CD69, along with the potent ability to produce TNF-α, CXCL-1, IL-2, and CCL-5, MZPs could potentially protect against TB by regulating systemic immune responses,[65,73,74,91] like MZB cells. For ABCs, our results showed that ABCs expanded in the lungs in response to infection (Figures 1G and 1H), consistent with their known presence in a variety of infectious diseases, including viral,[26]

bacterial,[31] and parasitic infections.[109–112] In line with other studies,[33,113] our results confirmed that ABCs exhibited strong cytokine production (Figures 5A–5J and S5B–S5K), indicating their regulatory role in immune responses in TB. Interestingly, ABCs have been shown to serve as memory B cells and mediate long-term protection in several infectious diseases.[31,32,114] In line with these findings, our results suggested that ABCs in TB displayed memory-like phenotype and served as a pool for accumulating memory-like B cells (Figures 3D and 3E). Furthermore, abundant CD69 expression on ABCs (Figures 3C and S4B) could facilitate their retention in lung tissues, suggesting that ABCs might serve as tissue-resident memory B cells, impacting the long-term course of the disease. In conclusion, MZPs and ABCs displayed functional phenotypes that were distinct from those of conventional B cells, characterized by either cytokine production or memory responses.

Reduction of Mtb reversed the accumulation and activation of MZB cells and other unconventional B cells (Figure 7), suggesting that the unconventional immune landscape was not sustained over the long term following successful treatment. Upon eradication of Mtb in the spleen at the end of chemotherapy, the accumulation and activation of MZB cells and other unconventional B cells returned to background levels, resembling the immune landscape in healthy mice (Figure S7B). This observation suggests that B cells abolish changes in the immune landscape after infection resolution. Enriched $CD95^+$ cells in MZB and MZP subsets could preferentially undergo activation-induced cell death when the infectious challenges diminished[115] (Figure S4F). The accumulation of MZB cells,[22,39–43,116,117] MZPs,[118,119] and ABCs[120,121] is associated with the onset of several autoimmune diseases. Eliminating the accumulation and activation of these cells potentially reduces the risk of triggering TB-related autoimmune diseases[122–125] after disease clearance. Therefore, our observations indicate that the rapid recovery of the B cell immune landscape after Mtb clearance may serve as a safety mechanism to mitigate the development of autoimmune diseases. On the other hand, we also observed that B cells continued displaying an unconventional landscape and expressing activation markers in response to the remaining Mtb burden in the lungs (Figures 7B–7E). This highlighted the sensitivity of B cells to a low Mtb burden. In a real-world context, Mtb can initiate infection and persist in the lungs at a very low burden,[126,127] implying that targeting these sensitive B cells may represent a potential vaccination strategy.

Our study provides the insight that leveraging the regulatory functions of MZB cells may offer a promising avenue for TB vaccine development. Historically, the primary strategy for TB vaccine development has been to elicit polyfunctional CD4 T cells,[95] which can shape cytokine patterns to create an anti-TB environment. Surprisingly, our results showed that MZB cells not only produced multiple cytokines and shaped cytokine patterns, like polyfunctional CD4 T cells, but also regulated the activities of innate and adaptive immune cells, orchestrating protection against TB. Therefore, enhancing MZB cell responses during BCG vaccination may improve vaccine efficacy by using their regulatory functions to shape optimal immune responses. Furthermore, activated and memory-like MZB cells may serve as tissue-resident memory B cells to provide long-term protection. The heightened sensitivity of the MZB cells potentially offered the ability to respond to a low burden of Mtb at the initial or latent stage of TB. In conclusion, our study suggests that, beyond solely focusing on antibody production, targeting regulatory functions of B cells can be a valuable strategy for TB vaccine development.

Limitations of the study

The blockade of CD11a and CD49d for depleting MZB cells can non-specifically affect other cell types in our *in vivo* system, limiting our interpretation regarding the role of MZB cells in TB. Given that various cell types express CD11a and CD49d, including B cells, T cells, NK cells, monocytes, neutrophils, eosinophils, and basophils,[128–130] the blockade may also influence these cells. For example, this blockade may inadvertently reduce the accumulation of NK and CD8 T cells in MZB-depleted mice. Furthermore, the blockade did not prevent the accumulation of pulmonary MZB cells, limiting our ability to assess their functions in the lungs during TB. Using genetically modified mice lacking MZB cells[131] can offer a strategy to avoid the non-specific interferences associated with antibody-mediated cell depletion. However, these genetically modified mouse models also possess functional deficiencies in various cell types. For example, Notch2-deficient mice reduce MZB cells[47] but concurrently impair the differentiation of $CD4^+$ T helper 2 cells,[132] cytotoxic CD8 T cells,[133] dendritic cells,[134] and mast cells.[135] Generally, examining the role of MZB cells in TB on different mouse models may provide a more complete picture and is the direction for future work.

STAR★METHODS

Detailed methods are provided in the online version of this paper and include the following:

- KEY RESOURCES TABLE
- RESOURCE AVAILABILITY
  - Lead contact
  - Materials availability
  - Data and code availability
- EXPERIMENTAL MODEL AND SUBJECT DETAILS
  - Mice and aerosol infection
  - Enumeration of tissue bacterial load
  - Preparation of single-cell suspensions
  - Flow cytometry
  - Antibodies and reagents for flow cytometry analysis
  - *Ex vivo* restimulation of cells
  - Cell sorting
  - Depletion of MZB cells
  - Antimycobacterial chemotherapy
  - Plasma sample collection
  - ELISA
  - Multiplex analysis of cytokines
  - Library preparation and RNA-Seq processing
  - Reads mapping and quantification
  - Immunostaining and confocal microscopy
- QUANTIFICATION AND STATISTICAL ANALYSIS

SUPPLEMENTAL INFORMATION

Supplemental information can be found online at https://doi.org/10.1016/j.celrep.2024.114426.

ACKNOWLEDGMENTS

We extend our gratitude to Dr. Paul Hutchinson and Teo Guo Hui for their guidance on flow cytometry and to Prof. Nick Paton for his scientific discussions. Our appreciation goes to Dr. Erika Shor and Frank Nuritdinov for their editorial support, Weiliang Chen for his BSL-3 operational management, and Melissa Cristaldo for performing cryosection. We also acknowledge the support of the BSL-3 Core Facility and Flow Cytometry Laboratory at NUS; the Flow Cytometry Core Facility, Research Animal Facility, and BSL-3 Facility at CDI; and the Immunogenomics Platform at Singapore Immunology Network (SIgN). We are thankful to the NIH Tetramer core facility for providing CD1d tetramer-APC (PSB-57) and to BEI Resources for supplying Mtb, H37Rv, gamma-irradiated whole cells (cat. no. NR-49098) and Mtb, H37Rv, whole cell lysate (cat. no. NR-14822). This work was supported by the National Medical Research Council Singapore under NMRC/CG/013/2013 to T.D. and NMRC/OFYIRG/0001/2016 to M.G.; SIgN, Agency for Science, Technology and Research (A*STAR) under other funding sources; and the National Institute of Allergy and Infectious Diseases of the National Institutes of Health under award nos. U19AI162568 and R01AI161013 to M.G. The content is solely the responsibility of the authors and does not necessarily represent the official views of the National Institutes of Health.

AUTHOR CONTRIBUTIONS

Conceptualization, C.-Y.T., K.F., and M.G.; methodology, C.-Y.T. and M.G.; software, A.A. and B.L.; validation, C.-Y.T. and M.G.; formal analysis, C.-Y.T. and A.A.; investigation, C.-Y.T., M.O., J.H.P., B.C.M.Y., J.J.J.L., and M.G.; resources, K.F., A.A., B.L., T.D., and M.G.; writing – original draft, C.-Y.T.; writing – review & editing, C.-Y.T., W.-S.T., K.F., and M.G.; visualization, C.-Y.T., W.-S.T., and A.A.; supervision, C.-Y.T., K.F., and M.G.; project administration, C.-Y.T. and M.G.; funding acquisition, T.D. and M.G.

DECLARATION OF INTERESTS

The authors declare no competing interests.

DECLARATION OF GENERATIVE AI AND AI-ASSISTED TECHNOLOGIES IN THE WRITING PROCESS

During the preparation of this work, the author used Grammarly and ChatGPT to check grammar, check spelling, and improve readability. After using this tool/service, the author reviewed and edited the content as needed and takes full responsibility for the content of the publication.

Received: December 14, 2023
Revised: April 29, 2024
Accepted: June 17, 2024
Published: July 2, 2024

REFERENCES

1. Bagcchi, S. (2023). WHO's Global Tuberculosis Report 2022. Lancet Microbe *4*, e20. https://doi.org/10.1016/S2666-5247(22)00359-7.
2. Andersen, P., and Doherty, T.M. (2005). The success and failure of BCG - implications for a novel tuberculosis vaccine. Nat. Rev. Microbiol. *3*, 656–662. https://doi.org/10.1038/nrmicro1211.
3. Leveton, C., Barnass, S., Champion, B., Lucas, S., De Souza, B., Nicol, M., Banerjee, D., and Rook, G. (1989). T-cell-mediated protection of mice against virulent Mycobacterium tuberculosis. Infect. Immun. *57*, 390–395. https://doi.org/10.1128/iai.57.2.390-395.1989.
4. Flory, C.M., Hubbard, R.D., and Collins, F.M. (1992). Effects of in vivo T lymphocyte subset depletion on mycobacterial infections in mice. J. Leukoc. Biol. *51*, 225–229. https://doi.org/10.1002/jlb.51.3.225.
5. Muller, I., Cobbold, S.P., Waldmann, H., and Kaufmann, S.H. (1987). Impaired resistance to Mycobacterium tuberculosis infection after selective in vivo depletion of L3T4+ and Lyt-2+ T cells. Infect. Immun. *55*, 2037–2041. https://doi.org/10.1128/iai.55.9.2037-2041.1987.
6. Orme, I.M. (1988). Characteristics and specificity of acquired immunologic memory to Mycobacterium tuberculosis infection. J. Immunol. *140*, 3589–3593.
7. Orme, I.M. (1987). The kinetics of emergence and loss of mediator T lymphocytes acquired in response to infection with Mycobacterium tuberculosis. J. Immunol. *138*, 293–298.
8. Behar, S.M., Dascher, C.C., Grusby, M.J., Wang, C.R., and Brenner, M.B. (1999). Susceptibility of mice deficient in CD1D or TAP1 to infection with Mycobacterium tuberculosis. J. Exp. Med. *189*, 1973–1980. https://doi.org/10.1084/jem.189.12.1973.
9. Flynn, J.L., Goldstein, M.M., Triebold, K.J., Koller, B., and Bloom, B.R. (1992). Major histocompatibility complex class I-restricted T cells are required for resistance to Mycobacterium tuberculosis infection. Proc. Natl. Acad. Sci. USA *89*, 12013–12017. https://doi.org/10.1073/pnas.89.24.12013.
10. Sousa, A.O., Mazzaccaro, R.J., Russell, R.G., Lee, F.K., Turner, O.C., Hong, S., Van Kaer, L., and Bloom, B.R. (2000). Relative contributions of distinct MHC class I-dependent cell populations in protection to tuberculosis infection in mice. Proc. Natl. Acad. Sci. USA *97*, 4204–4208. https://doi.org/10.1073/pnas.97.8.4204.
11. Maglione, P.J., Xu, J., and Chan, J. (2007). B cells moderate inflammatory progression and enhance bacterial containment upon pulmonary challenge with Mycobacterium tuberculosis. J. Immunol. *178*, 7222–7234. https://doi.org/10.4049/jimmunol.178.11.7222.
12. Kozakiewicz, L., Chen, Y., Xu, J., Wang, Y., Dunussi-Joannopoulos, K., Ou, Q., Flynn, J.L., Porcelli, S.A., Jacobs, W.R., Jr., and Chan, J. (2013). B cells regulate neutrophilia during Mycobacterium tuberculosis infection and BCG vaccination by modulating the interleukin-17 response. PLoS Pathog. *9*, e1003472. https://doi.org/10.1371/journal.ppat.1003472.
13. Vordermeier, H.M., Venkataprasad, N., Harris, D.P., and Ivanyi, J. (2003). Increase of tuberculous infection in the organs of B cell-deficient mice. Clin. Exp. Immunol. *106*, 312–316. https://doi.org/10.1046/j.1365-2249.1996.d01-845.x.
14. Linge, I., Kondratieva, E., and Apt, A. (2023). Prolonged B-Lymphocyte-Mediated Immune and Inflammatory Responses to Tuberculosis Infection in the Lungs of TB-Resistant Mice. Int. J. Mol. Sci. *24*, 1140. https://doi.org/10.3390/ijms24021140.
15. Phuah, J., Wong, E.A., Gideon, H.P., Maiello, P., Coleman, M.T., Hendricks, M.R., Ruden, R., Cirrincione, L.R., Chan, J., Lin, P.L., and Flynn, J.L. (2016). Effects of B Cell Depletion on Early Mycobacterium tuberculosis Infection in Cynomolgus Macaques. Infect. Immun. *84*, 1301–1311. https://doi.org/10.1128/IAI.00083-16.
16. Bosio, C.M., Gardner, D., and Elkins, K.L. (2000). Infection of B cell-deficient mice with CDC 1551, a clinical isolate of Mycobacterium tuberculosis: delay in dissemination and development of lung pathology. J. Immunol. *164*, 6417–6425. https://doi.org/10.4049/jimmunol.164.12.6417.
17. Torrado, E., Fountain, J.J., Robinson, R.T., Martino, C.A., Pearl, J.E., Rangel-Moreno, J., Tighe, M., Dunn, R., and Cooper, A.M. (2013). Differential and site specific impact of B cells in the protective immune response to Mycobacterium tuberculosis in the mouse. PLoS One *8*, e61681. https://doi.org/10.1371/journal.pone.0061681.
18. Johnson, C.M., Cooper, A.M., Frank, A.A., Bonorino, C., Wysoki, L.J., and Orme, I.M. (1997). Mycobacterium tuberculosis aerogenic rechallenge infections in B cell-deficient mice. Tuber. Lung Dis. *78*, 257–261. https://doi.org/10.1016/s0962-8479(97)90006-x.
19. Allman, D., and Pillai, S. (2008). Peripheral B cell subsets. Curr. Opin. Immunol. *20*, 149–157. https://doi.org/10.1016/j.coi.2008.03.014.
20. Baumgarth, N. (2004). B-cell immunophenotyping. Methods Cell Biol. *75*, 643–662. https://doi.org/10.1016/s0091-679x(04)75027-x.

21. Baumgarth, N. (2011). The double life of a B-1 cell: self-reactivity selects for protective effector functions. Nat. Rev. Immunol. *11*, 34–46. https://doi.org/10.1038/nri2901.

22. Palm, A.K.E., Friedrich, H.C., and Kleinau, S. (2016). Nodal marginal zone B cells in mice: a novel subset with dormant self-reactivity. Sci. Rep. *6*, 27687. https://doi.org/10.1038/srep27687.

23. Huang, Y., Getahun, A., Heiser, R.A., Detanico, T.O., Aviszus, K., Kirchenbaum, G.A., Casper, T.L., Huang, C., Aydintug, M.K., Carding, S.R., et al. (2016). γδ T Cells Shape Preimmune Peripheral B Cell Populations. J. Immunol. *196*, 217–231. https://doi.org/10.4049/jimmunol.1501064.

24. Hoffman, W., Lakkis, F.G., and Chalasani, G. (2016). B Cells, Antibodies, and More. Clin. J. Am. Soc. Nephrol. *11*, 137–154. https://doi.org/10.2215/CJN.09430915.

25. Mouat, I.C., and Horwitz, M.S. (2022). Age-associated B cells in viral infection. PLoS Pathog. *18*, e1010297. https://doi.org/10.1371/journal.ppat.1010297.

26. Cancro, M.P. (2020). Age-Associated B Cells. Annu. Rev. Immunol. *38*, 315–340. https://doi.org/10.1146/annurev-immunol-092419-031130.

27. Knox, J.J., Myles, A., and Cancro, M.P. (2019). T-bet(+) memory B cells: Generation, function, and fate. Immunol. Rev. *288*, 149–160. https://doi.org/10.1111/imr.12736.

28. Cerutti, A., Cols, M., and Puga, I. (2013). Marginal zone B cells: virtues of innate-like antibody-producing lymphocytes. Nat. Rev. Immunol. *13*, 118–132. https://doi.org/10.1038/nri3383.

29. Zouali, M., and Richard, Y. (2011). Marginal zone B-cells, a gatekeeper of innate immunity. Front. Immunol. *2*, 63. https://doi.org/10.3389/fimmu.2011.00063.

30. Srivastava, B., Quinn, W.J., 3rd, Hazard, K., Erikson, J., and Allman, D. (2005). Characterization of marginal zone B cell precursors. J. Exp. Med. *202*, 1225–1234. https://doi.org/10.1084/jem.20051038.

31. Racine, R., Chatterjee, M., and Winslow, G.M. (2008). CD11c expression identifies a population of extrafollicular antigen-specific splenic plasmablasts responsible for CD4 T-independent antibody responses during intracellular bacterial infection. J. Immunol. *181*, 1375–1385. https://doi.org/10.4049/jimmunol.181.2.1375.

32. Yates, J.L., Racine, R., McBride, K.M., and Winslow, G.M. (2013). T cell-dependent IgM memory B cells generated during bacterial infection are required for IgG responses to antigen challenge. J. Immunol. *191*, 1240–1249. https://doi.org/10.4049/jimmunol.1300062.

33. Joosten, S.A., van Meijgaarden, K.E., Del Nonno, F., Baiocchini, A., Petrone, L., Vanini, V., Smits, H.H., Palmieri, F., Goletti, D., and Ottenhoff, T.H.M. (2016). Patients with Tuberculosis Have a Dysfunctional Circulating B-Cell Compartment, Which Normalizes following Successful Treatment. PLoS Pathog. *12*, e1005687. https://doi.org/10.1371/journal.ppat.1005687.

34. du Plessis, W.J., Keyser, A., Walzl, G., and Loxton, A.G. (2016). Phenotypic analysis of peripheral B cell populations during Mycobacterium tuberculosis infection and disease. J. Inflamm. *13*, 23. https://doi.org/10.1186/s12950-016-0133-4.

35. Linge, I., Dyatlov, A., Kondratieva, E., Avdienko, V., Apt, A., and Kondratieva, T. (2017). B-lymphocytes forming follicle-like structures in the lung tissue of tuberculosis-infected mice: Dynamics, phenotypes and functional activity. Tuberculosis *102*, 16–23. https://doi.org/10.1016/j.tube.2016.11.005.

36. Girma, T., Tsegaye, A., Desta, K., Ayalew, S., Tamene, W., Zewdie, M., Howe, R., and Mihret, A. (2023). Phenotypic characterization of Peripheral B cells in Mycobacterium tuberculosis infection and disease in Addis Ababa, Ethiopia. Tuberculosis *140*, 102329. https://doi.org/10.1016/j.tube.2023.102329.

37. Dick, T., Manjunatha, U., Kappes, B., and Gengenbacher, M. (2010). Vitamin B6 biosynthesis is essential for survival and virulence of Mycobacterium tuberculosis. Mol. Microbiol. *78*, 980–988. https://doi.org/10.1111/j.1365-2958.2010.07381.x.

38. Prokopec, K.E., Georgoudaki, A.M., Sohn, S., Wermeling, F., Grönlund, H., Lindh, E., Carroll, M.C., and Karlsson, M.C.I. (2016). Cutting Edge: Marginal Zone Macrophages Regulate Antigen Transport by B Cells to the Follicle in the Spleen via CD21. J. Immunol. *197*, 2063–2068. https://doi.org/10.4049/jimmunol.1502282.

39. Marino, E., Batten, M., Groom, J., Walters, S., Liuwantara, D., Mackay, F., and Grey, S.T. (2008). Marginal-zone B-cells of nonobese diabetic mice expand with diabetes onset, invade the pancreatic lymph nodes, and present autoantigen to diabetogenic T-cells. Diabetes *57*, 395–404. https://doi.org/10.2337/db07-0589.

40. Li, J., Kuzin, I., Moshkani, S., Proulx, S.T., Xing, L., Skrombolas, D., Dunn, R., Sanz, I., Schwarz, E.M., and Bottaro, A. (2010). Expanded CD23(+)/CD21(hi) B cells in inflamed lymph nodes are associated with the onset of inflammatory-erosive arthritis in TNF-transgenic mice and are targets of anti-CD20 therapy. J. Immunol. *184*, 6142–6150. https://doi.org/10.4049/jimmunol.0903489.

41. Moshkani, S., Kuzin, I.I., Adewale, F., Jansson, J., Sanz, I., Schwarz, E.M., and Bottaro, A. (2012). CD23+ CD21(high) CD1d(high) B cells in inflamed lymph nodes are a locally differentiated population with increased antigen capture and activation potential. J. Immunol. *188*, 5944–5953. https://doi.org/10.4049/jimmunol.1103071.

42. Groom, J., Kalled, S.L., Cutler, A.H., Olson, C., Woodcock, S.A., Schneider, P., Tschopp, J., Cachero, T.G., Batten, M., Wheway, J., et al. (2002). Association of BAFF/BLyS overexpression and altered B cell differentiation with Sjögren's syndrome. J. Clin. Invest. *109*, 59–68. https://doi.org/10.1172/JCI14121.

43. Batten, M., Groom, J., Cachero, T.G., Qian, F., Schneider, P., Tschopp, J., Browning, J.L., and Mackay, F. (2000). BAFF mediates survival of peripheral immature B lymphocytes. J. Exp. Med. *192*, 1453–1466. https://doi.org/10.1084/jem.192.10.1453.

44. Khader, S.A., Guglani, L., Rangel-Moreno, J., Gopal, R., Fallert Junecko, B.A., Fountain, J.J., Martino, C., Pearl, J.E., Tighe, M., Lin, Y.Y., et al. (2011). IL-23 is required for long-term control of Mycobacterium tuberculosis and B cell follicle formation in the infected lung. J. Immunol. *187*, 5402–5407. https://doi.org/10.4049/jimmunol.1101377.

45. Kahnert, A., Höpken, U., Stein, M., Bandermann, S., Lipp, M., and Kaufmann, S. (2007). Mycobacterium tuberculosis triggers formation of lymphoid structure in murine lungs. J. Infect. Dis. *195*, 46–54. https://doi.org/10.1086/508894.

46. Won, W.J., and Kearney, J.F. (2002). CD9 is a unique marker for marginal zone B cells, B1 cells, and plasma cells in mice. J. Immunol. *168*, 5605–5611. https://doi.org/10.4049/jimmunol.168.11.5605.

47. Lechner, M., Engleitner, T., Babushku, T., Schmidt-Supprian, M., Rad, R., Strobl, L.J., and Zimber-Strobl, U. (2021). Notch2-mediated plasticity between marginal zone and follicular B cells. Nat. Commun. *12*, 1111. https://doi.org/10.1038/s41467-021-21359-1.

48. Weisel, N.M., Joachim, S.M., Smita, S., Callahan, D., Elsner, R.A., Conter, L.J., Chikina, M., Farber, D.L., Weisel, F.J., and Shlomchik, M.J. (2022). Surface phenotypes of naive and memory B cells in mouse and human tissues. Nat. Immunol. *23*, 135–145. https://doi.org/10.1038/s41590-021-01078-x.

49. Garraud, O., Borhis, G., Badr, G., Degrelle, S., Pozzetto, B., Cognasse, F., and Richard, Y. (2012). Revisiting the B-cell compartment in mouse and humans: more than one B-cell subset exists in the marginal zone and beyond. BMC Immunol. *13*, 63. https://doi.org/10.1186/1471-2172-13-63.

50. Xu, S., Tan, J.E.L., Wong, E.P.Y., Manickam, A., Ponniah, S., and Lam, K.P. (2000). B cell development and activation defects resulting in xid-like immunodeficiency in BLNK/SLP-65-deficient mice. Int. Immunol. *12*, 397–404. https://doi.org/10.1093/intimm/12.3.397.

51. Lenschow, D.J., Sperling, A.I., Cooke, M.P., Freeman, G., Rhee, L., Decker, D.C., Gray, G., Nadler, L.M., Goodnow, C.C., and Bluestone, J.A. (1994). Differential up-regulation of the B7-1 and B7-2 costimulatory

molecules after Ig receptor engagement by antigen. J. Immunol. *153*, 1990–1997.

52. Sharpe, A.H., and Freeman, G.J. (2002). The B7-CD28 superfamily. Nat. Rev. Immunol. *2*, 116–126. https://doi.org/10.1038/nri727.
53. Collins, M., Ling, V., and Carreno, B.M. (2005). The B7 family of immune-regulatory ligands. Genome Biol. *6*, 223. https://doi.org/10.1186/gb-2005-6-6-223.
54. Shiow, L.R., Rosen, D.B., Brdičková, N., Xu, Y., An, J., Lanier, L.L., Cyster, J.G., and Matloubian, M. (2006). CD69 acts downstream of interferon-α/β to inhibit S1P1 and lymphocyte egress from lymphoid organs. Nature *440*, 540–544. https://doi.org/10.1038/nature04606.
55. Zuccarino-Catania, G.V., Sadanand, S., Weisel, F.J., Tomayko, M.M., Meng, H., Kleinstein, S.H., Good-Jacobson, K.L., and Shlomchik, M.J. (2014). CD80 and PD-L2 define functionally distinct memory B cell subsets that are independent of antibody isotype. Nat. Immunol. *15*, 631–637. https://doi.org/10.1038/ni.2914.
56. Bergmann, B., Grimsholm, O., Thorarinsdottir, K., Ren, W., Jirholt, P., Gjertsson, I., and Mårtensson, I. (2013). Memory B cells in mouse models. Scand. J. Immunol. *78*, 149–156. https://doi.org/10.1111/sji.12073.
57. Anderson, S.M., Tomayko, M.M., Ahuja, A., Haberman, A.M., and Shlomchik, M.J. (2007). New markers for murine memory B cells that define mutated and unmutated subsets. J. Exp. Med. *204*, 2103–2114. https://doi.org/10.1084/jem.20062571.
58. Obukhanych, T.V., and Nussenzweig, M.C. (2006). T-independent type II immune responses generate memory B cells. J. Exp. Med. *203*, 305–310. https://doi.org/10.1084/jem.20052036.
59. Dogan, I., Bertocci, B., Vilmont, V., Delbos, F., Mégret, J., Storck, S., Reynaud, C.A., and Weill, J.C. (2009). Multiple layers of B cell memory with different effector functions. Nat. Immunol. *10*, 1292–1299. https://doi.org/10.1038/ni.1814.
60. Lu, T.T., and Cyster, J.G. (2002). Integrin-mediated long-term B cell retention in the splenic marginal zone. Science *297*, 409–412. https://doi.org/10.1126/science.1071632.
61. Belperron, A.A., Dailey, C.M., Booth, C.J., and Bockenstedt, L.K. (2007). Marginal zone B-cell depletion impairs murine host defense against Borrelia burgdorferi infection. Infect. Immun. *75*, 3354–3360. https://doi.org/10.1128/IAI.00422-07.
62. Bankoti, R., Gupta, K., Levchenko, A., and Stäger, S. (2012). Marginal zone B cells regulate antigen-specific T cell responses during infection. J. Immunol. *188*, 3961–3971. https://doi.org/10.4049/jimmunol.1102880.
63. Zerra, P.E., Cox, C., Baldwin, W.H., Patel, S.R., Arthur, C.M., Lollar, P., Meeks, S.L., and Stowell, S.R. (2017). Marginal zone B cells are critical to factor VIII inhibitor formation in mice with hemophilia A. Blood *130*, 2559–2568. https://doi.org/10.1182/blood-2017-05-782912.
64. Shen, P., and Fillatreau, S. (2015). Antibody-independent functions of B cells: a focus on cytokines. Nat. Rev. Immunol. *15*, 441–451. https://doi.org/10.1038/nri3857.
65. Flynn, J.L., Goldstein, M.M., Chan, J., Triebold, K.J., Pfeffer, K., Lowenstein, C.J., Schrelber, R., Mak, T.W., and Bloom, B.R. (1995). Tumor necrosis factor-alpha is required in the protective immune response against Mycobacterium tuberculosis in mice. Immunity *2*, 561–572. https://doi.org/10.1016/1074-7613(95)90001-2.
66. Keane, J., Gershon, S., Wise, R.P., Mirabile-Levens, E., Kasznica, J., Schwieterman, W.D., Siegel, J.N., and Braun, M.M. (2001). Tuberculosis associated with infliximab, a tumor necrosis factor alpha-neutralizing agent. N. Engl. J. Med. *345*, 1098–1104. https://doi.org/10.1056/NEJMoa011110.
67. Vesosky, B., Rottinghaus, E.K., Stromberg, P., Turner, J., and Beamer, G. (2010). CCL5 participates in early protection against Mycobacterium tuberculosis. J. Leukoc. Biol. *87*, 1153–1165. https://doi.org/10.1189/jlb.1109742.
68. Chen, C.Y., Huang, D., Yao, S., Halliday, L., Zeng, G., Wang, R.C., and Chen, Z.W. (2012). IL-2 simultaneously expands Foxp3+ T regulatory and T effector cells and confers resistance to severe tuberculosis (TB): implicative Treg-T effector cooperation in immunity to TB. J. Immunol. *188*, 4278–4288. https://doi.org/10.4049/jimmunol.1101291.
69. Toossi, Z., Kleinhenz, M.E., and Ellner, J.J. (1986). Defective interleukin 2 production and responsiveness in human pulmonary tuberculosis. J. Exp. Med. *163*, 1162–1172. https://doi.org/10.1084/jem.163.5.1162.
70. Gonzalez-Juarrero, M., Hattle, J.M., Izzo, A., Junqueira-Kipnis, A.P., Shim, T.S., Trapnell, B.C., Cooper, A.M., and Orme, I.M. (2005). Disruption of granulocyte macrophage-colony stimulating factor production in the lungs severely affects the ability of mice to control Mycobacterium tuberculosis infection. J. Leukoc. Biol. *77*, 914–922. https://doi.org/10.1189/jlb.1204723.
71. Szeliga, J., Daniel, D.S., Yang, C.H., Sever-Chroneos, Z., Jagannath, C., and Chroneos, Z.C. (2008). Granulocyte-macrophage colony stimulating factor-mediated innate responses in tuberculosis. Tuberculosis *88*, 7–20. https://doi.org/10.1016/j.tube.2007.08.009.
72. Mishra, A., Singh, V.K., Actor, J.K., Hunter, R.L., Jagannath, C., Subbian, S., and Khan, A. (2020). GM-CSF Dependent Differential Control of Mycobacterium tuberculosis Infection in Human and Mouse Macrophages: Is Macrophage Source of GM-CSF Critical to Tuberculosis Immunity? Front. Immunol. *11*, 1599. https://doi.org/10.3389/fimmu.2020.01599.
73. Boro, M., and Balaji, K.N. (2017). CXCL1 and CXCL2 Regulate NLRP3 Inflammasome Activation via G-Protein-Coupled Receptor CXCR2. J. Immunol. *199*, 1660–1671. https://doi.org/10.4049/jimmunol.1700129.
74. Boro, M., Singh, V., and Balaji, K.N. (2016). Mycobacterium tuberculosis-triggered Hippo pathway orchestrates CXCL1/2 expression to modulate host immune responses. Sci. Rep. *6*, 37695. https://doi.org/10.1038/srep37695.
75. Beamer, G.L., Flaherty, D.K., Assogba, B.D., Stromberg, P., Gonzalez-Juarrero, M., de Waal Malefyt, R., Vesosky, B., and Turner, J. (2008). Interleukin-10 promotes Mycobacterium tuberculosis disease progression in CBA/J mice. J. Immunol. *181*, 5545–5550. https://doi.org/10.4049/jimmunol.181.8.5545.
76. Redford, P.S., Boonstra, A., Read, S., Pitt, J., Graham, C., Stavropoulos, E., Bancroft, G.J., and O'Garra, A. (2010). Enhanced protection to Mycobacterium tuberculosis infection in IL-10-deficient mice is accompanied by early and enhanced Th1 responses in the lung. Eur. J. Immunol. *40*, 2200–2210. https://doi.org/10.1002/eji.201040433.
77. Redford, P.S., Murray, P.J., and O'Garra, A. (2011). The role of IL-10 in immune regulation during M. tuberculosis infection. Mucosal Immunol. *4*, 261–270. https://doi.org/10.1038/mi.2011.7.
78. Buccheri, S., Reljic, R., Caccamo, N., Ivanyi, J., Singh, M., Salerno, A., and Dieli, F. (2007). IL-4 depletion enhances host resistance and passive IgA protection against tuberculosis infection in BALB/c mice. Eur. J. Immunol. *37*, 729–737. https://doi.org/10.1002/eji.200636764.
79. Hernandez-Pando, R., Aguilar, D., Hernandez, M., Orozco, H., and Rook, G. (2004). Pulmonary tuberculosis in BALB/c mice with non-functional IL-4 genes: changes in the inflammatory effects of TNF-alpha and in the regulation of fibrosis. Eur. J. Immunol. *34*, 174–183. https://doi.org/10.1002/eji.200324253.
80. Pooran, A., Davids, M., Nel, A., Shoko, A., Blackburn, J., and Dheda, K. (2019). IL-4 subverts mycobacterial containment in Mycobacterium tuberculosis-infected human macrophages. Eur. Respir. J. *54*, 1802242. https://doi.org/10.1183/13993003.02242-2018.
81. Candolfi, M., Curtin, J.F., Yagiz, K., Assi, H., Wibowo, M.K., Alzadeh, G.E., Foulad, D., Muhammad, A.G., Salehi, S., Keech, N., et al. (2011). B cells are critical to T-cell-mediated antitumor immunity induced by a combined immune-stimulatory/conditionally cytotoxic therapy for glioblastoma. Neoplasia *13*, 947–IN23. https://doi.org/10.1593/neo.11024.
82. Lo, L.W., Chang, C.W., Chiang, M.F., Lin, I.Y., and Lin, K.I. (2021). Marginal Zone B Cells Assist With Neutrophil Accumulation to Fight Against

Systemic Staphylococcus aureus Infection. Front. Immunol. *12*, 636818. https://doi.org/10.3389/fimmu.2021.636818.

83. Lee, C.C., and Kung, J.T. (2012). Marginal zone B cell is a major source of Il-10 in Listeria monocytogenes susceptibility. J. Immunol. *189*, 3319–3327. https://doi.org/10.4049/jimmunol.1201247.

84. Martin, F., Oliver, A.M., and Kearney, J.F. (2001). Marginal zone and B1 B cells unite in the early response against T-independent blood-borne particulate antigens. Immunity *14*, 617–629. https://doi.org/10.1016/s1074-7613(01)00129-7.

85. Gatto, D., Ruedl, C., Odermatt, B., and Bachmann, M.F. (2004). Rapid response of marginal zone B cells to viral particles. J. Immunol. *173*, 4308–4316. https://doi.org/10.4049/jimmunol.173.7.4308.

86. Vinuesa, C.G., Sze, D., Cook, M.C., Toellner, K.M., Klaus, G., Ball, J., and MacLennan, I. (2003). Recirculating and germinal center B cells differentiate into cells responsive to polysaccharide antigens. Eur. J. Immunol. *33*, 297–305. https://doi.org/10.1002/immu.200310003.

87. Nandi, D., Gross, J.A., and Allison, J.P. (1994). CD28-mediated costimulation is necessary for optimal proliferation of murine NK cells. J. Immunol. *152*, 3361–3369.

88. Bhatt, K., Uzelac, A., Mathur, S., McBride, A., Potian, J., and Salgame, P. (2009). B7 costimulation is critical for host control of chronic Mycobacterium tuberculosis infection. J. Immunol. *182*, 3793–3800. https://doi.org/10.4049/jimmunol.0802996.

89. Bhatt, K., Kim, A., Kim, A., Mathur, S., and Salgame, P. (2013). Equivalent functions for B7.1 and B7.2 costimulation in mediating host resistance to Mycobacterium tuberculosis. Cell. Immunol. *285*, 69–75. https://doi.org/10.1016/j.cellimm.2013.09.004.

90. Barker, K.A., Etesami, N.S., Shenoy, A.T., Arafa, E.I., de Ana, C.L., Smith, N.M., Martin, I.M., Goltry, W.N., Barron, A.M., Browning, J.L., et al. (2021). Lung-resident memory B cells protect against bacterial pneumonia. J. Clin. Invest. *131*, e141810. https://doi.org/10.1172/JCI141810.

91. Mehta, A.K., Gracias, D.T., and Croft, M. (2018). TNF activity and T cells. Cytokine *101*, 14–18. https://doi.org/10.1016/j.cyto.2016.08.003.

92. Liao, W., Lin, J.X., and Leonard, W.J. (2013). Interleukin-2 at the crossroads of effector responses, tolerance, and immunotherapy. Immunity *38*, 13–25. https://doi.org/10.1016/j.immuni.2013.01.004.

93. Rothchild, A.C., Stowell, B., Goyal, G., Nunes-Alves, C., Yang, Q., Papavinasasundaram, K., Sassetti, C.M., Dranoff, G., Chen, X., Lee, J., and Behar, S.M. (2017). Role of Granulocyte-Macrophage Colony-Stimulating Factor Production by T Cells during Mycobacterium tuberculosis Infection. mBio *8*, e01514-17. https://doi.org/10.1128/mBio.01514-17.

94. Rothchild, A.C., Jayaraman, P., Nunes-Alves, C., and Behar, S.M. (2014). iNKT cell production of GM-CSF controls Mycobacterium tuberculosis. PLoS Pathog. *10*, e1003805. https://doi.org/10.1371/journal.ppat.1003805.

95. Lewinsohn, D.A., Lewinsohn, D.M., and Scriba, T.J. (2017). Polyfunctional CD4(+) T Cells As Targets for Tuberculosis Vaccination. Front. Immunol. *8*, 1262. https://doi.org/10.3389/fimmu.2017.01262.

96. Chen, Y., Bharrhan, S., Xu, J., Sharma, T., Wang, Y., Salgame, P., Zhang, J., Nargan, K., Steyn, A.J.C., Maglione, P.J., and Chan, J. (2023). B cells promote granulomatous inflammation during chronic Mycobacterium tuberculosis infection in mice. PLoS Pathog. *19*, e1011187. https://doi.org/10.1371/journal.ppat.1011187.

97. Garcia-Ferreras, R., Osuna-Perez, J., Ramirez-Santiago, G., Mendez-Perez, A., Acosta-Moreno, A.M., Del Campo, L., Gomez-Sanchez, M.J., Iborra, M., Herrero-Fernandez, B., Gonzalez-Granado, J.M., et al. (2023). Bacteria-instructed B cells cross-prime naive CD8(+) T cells triggering effective cytotoxic responses. EMBO Rep. *24*, e56131. https://doi.org/10.15252/embr.202256131.

98. Leadbetter, E.A., and Karlsson, M.C.I. (2021). Invariant natural killer T cells balance B cell immunity. Immunol. Rev. *299*, 93–107. https://doi.org/10.1111/imr.12938.

99. Barber, D.L., Mayer-Barber, K.D., Feng, C.G., Sharpe, A.H., and Sher, A. (2011). CD4 T cells promote rather than control tuberculosis in the absence of PD-1-mediated inhibition. J. Immunol. *186*, 1598–1607. https://doi.org/10.4049/jimmunol.1003304.

100. O'Garra, A., Redford, P.S., McNab, F.W., Bloom, C.I., Wilkinson, R.J., and Berry, M.P. (2013). The immune response in tuberculosis. Annu. Rev. Immunol. *31*, 475–527. https://doi.org/10.1146/annurev-immunol-032712-095939.

101. Cui, A., Huang, T., Li, S., Ma, A., Pérez, J.L., Sander, C., Keskin, D.B., Wu, C.J., Fraenkel, E., and Hacohen, N. (2024). Dictionary of immune responses to cytokines at single-cell resolution. Nature *625*, 377–384. https://doi.org/10.1038/s41586-023-06816-9.

102. Coquet, J.M., Chakravarti, S., Kyparissoudis, K., McNab, F.W., Pitt, L.A., McKenzie, B.S., Berzins, S.P., Smyth, M.J., and Godfrey, D.I. (2008). Diverse cytokine production by NKT cell subsets and identification of an IL-17-producing CD4-NK1.1- NKT cell population. Proc. Natl. Acad. Sci. USA *105*, 11287–11292. https://doi.org/10.1073/pnas.0801631105.

103. Irvine, E.B., O'Neil, A., Darrah, P.A., Shin, S., Choudhary, A., Li, W., Honnen, W., Mehra, S., Kaushal, D., Gideon, H.P., et al. (2021). Robust IgM responses following intravenous vaccination with Bacille Calmette–Guérin associate with prevention of Mycobacterium tuberculosis infection in macaques. Nat. Immunol. *22*, 1515–1523. https://doi.org/10.1038/s41590-021-01066-1.

104. Lang, K.S., Lang, P.A., Meryk, A., Pandyra, A.A., Boucher, L.M., Pozdeev, V.I., Tusche, M.W., Göthert, J.R., Haight, J., Wakeham, A., et al. (2013). Involvement of Toso in activation of monocytes, macrophages, and granulocytes. Proc. Natl. Acad. Sci. USA *110*, 2593–2598. https://doi.org/10.1073/pnas.1222264110.

105. Yu, J., Duong, V.H.H., Westphal, K., Westphal, A., Suwandi, A., Grassl, G.A., Brand, K., Chan, A.C., Föger, N., and Lee, K.H. (2018). Surface receptor Toso controls B cell-mediated regulation of T cell immunity. J. Clin. Invest. *128*, 1820–1836. https://doi.org/10.1172/JCI97280.

106. Liu, J., Zhu, H., Qian, J., Xiong, E., Zhang, L., Wang, Y.Q., Chu, Y., Kubagawa, H., Tsubata, T., and Wang, J.Y. (2018). Fcμ Receptor Promotes the Survival and Activation of Marginal Zone B Cells and Protects Mice against Bacterial Sepsis. Front. Immunol. *9*, 160. https://doi.org/10.3389/fimmu.2018.00160.

107. Lang, P.A., Meryk, A., Pandyra, A.A., Brenner, D., Brüstle, A., Xu, H.C., Merches, K., Lang, F., Khairnar, V., Sharma, P., et al. (2015). Toso regulates differentiation and activation of inflammatory dendritic cells during persistence-prone virus infection. Cell Death Differ. *22*, 164–173. https://doi.org/10.1038/cdd.2014.138.

108. Li, H., and Javid, B. (2018). Antibodies and tuberculosis: finally coming of age? Nat. Rev. Immunol. *18*, 591–596. https://doi.org/10.1038/s41577-018-0028-0.

109. Racine, R., McLaughlin, M., Jones, D.D., Wittmer, S.T., MacNamara, K.C., Woodland, D.L., and Winslow, G.M. (2011). IgM production by bone marrow plasmablasts contributes to long-term protection against intracellular bacterial infection. J. Immunol. *186*, 1011–1021. https://doi.org/10.4049/jimmunol.1002836.

110. Holla, P., Dizon, B., Ambegaonkar, A.A., Rogel, N., Goldschmidt, E., Boddapati, A.K., Sohn, H., Sturdevant, D., Austin, J.W., Kardava, L., et al. (2021). Shared transcriptional profiles of atypical B cells suggest common drivers of expansion and function in malaria, HIV, and autoimmunity. Sci. Adv. *7*, eabg8384. https://doi.org/10.1126/sciadv.abg8384.

111. Obeng-Adjei, N., Portugal, S., Holla, P., Li, S., Sohn, H., Ambegaonkar, A., Skinner, J., Bowyer, G., Doumbo, O.K., Traore, B., et al. (2017). Malaria-induced interferon-gamma drives the expansion of Tbethi atypical memory B cells. PLoS Pathog. *13*, e1006576. https://doi.org/10.1371/journal.ppat.1006576.

112. Weiss, G.E., Crompton, P.D., Li, S., Walsh, L.A., Moir, S., Traore, B., Kayentao, K., Ongoiba, A., Doumbo, O.K., and Pierce, S.K. (2009). Atypical memory B cells are greatly expanded in individuals living in a

malaria-endemic area. J. Immunol. *183*, 2176–2182. https://doi.org/10.4049/jimmunol.0901297.

113. Silva, C.S., Sundling, C., Folkesson, E., Fröberg, G., Nobrega, C., Canto-Gomes, J., Chambers, B.J., Lakshmikanth, T., Brodin, P., Bruchfeld, J., et al. (2021). High Dimensional Immune Profiling Reveals Different Response Patterns in Active and Latent Tuberculosis Following Stimulation With Mycobacterial Glycolipids. Front. Immunol. *12*, 727300. https://doi.org/10.3389/fimmu.2021.727300.
114. Stone, S.L., Peel, J.N., Scharer, C.D., Risley, C.A., Chisolm, D.A., Schultz, M.D., Yu, B., Ballesteros-Tato, A., Wojciechowski, W., Mousseau, B., et al. (2019). T-bet Transcription Factor Promotes Antibody-Secreting Cell Differentiation by Limiting the Inflammatory Effects of IFN-gamma on B Cells. Immunity *50*, 1172–1187.e7. https://doi.org/10.1016/j.immuni.2019.04.004.
115. Strasser, A., Jost, P.J., and Nagata, S. (2009). The many roles of FAS receptor signaling in the immune system. Immunity *30*, 180–192. https://doi.org/10.1016/j.immuni.2009.01.001.
116. Palm, A.K.E., Friedrich, H.C., Mezger, A., Salomonsson, M., Myers, L.K., and Kleinau, S. (2015). Function and regulation of self-reactive marginal zone B cells in autoimmune arthritis. Cell. Mol. Immunol. *12*, 493–504. https://doi.org/10.1038/cmi.2015.37.
117. Palm, A.K.E., and Kleinau, S. (2021). Marginal zone B cells: From housekeeping function to autoimmunity? J. Autoimmun. *119*, 102627. https://doi.org/10.1016/j.jaut.2021.102627.
118. Evans, J.G., Chavez-Rueda, K.A., Eddaoudi, A., Meyer-Bahlburg, A., Rawlings, D.J., Ehrenstein, M.R., and Mauri, C. (2007). Novel suppressive function of transitional 2 B cells in experimental arthritis. J. Immunol. *178*, 7868–7878. https://doi.org/10.4049/jimmunol.178.12.7868.
119. Kuzin, I.I., Kates, S.L., Ju, Y., Zhang, L., Rahimi, H., Wojciechowski, W., Bernstein, S.H., Burack, R., Schwarz, E.M., and Bottaro, A. (2016). Increased numbers of CD23(+) CD21(hi) Bin-like B cells in human reactive and rheumatoid arthritis lymph nodes. Eur. J. Immunol. *46*, 1752–1757. https://doi.org/10.1002/eji.201546266.
120. Rubtsov, A.V., Marrack, P., and Rubtsova, K. (2017). T-bet expressing B cells - Novel target for autoimmune therapies? Cell. Immunol. *321*, 35–39. https://doi.org/10.1016/j.cellimm.2017.04.011.
121. Mouat, I.C., Goldberg, E., and Horwitz, M.S. (2022). Age-associated B cells in autoimmune diseases. Cell. Mol. Life Sci. *79*, 402. https://doi.org/10.1007/s00018-022-04433-9.
122. Elkington, P., Tebruegge, M., and Mansour, S. (2016). Tuberculosis: An Infection-Initiated Autoimmune Disease? Trends Immunol. *37*, 815–818. https://doi.org/10.1016/j.it.2016.09.007.
123. Pigrau-Serrallach, C., and Rodríguez-Pardo, D. (2013). Bone and joint tuberculosis. Eur. Spine J. *22*, 556–566. https://doi.org/10.1007/s00586-012-2331-y.
124. Kakumanu, P., Yamagata, H., Sobel, E.S., Reeves, W.H., Chan, E.K.L., and Satoh, M. (2008). Patients with pulmonary tuberculosis are frequently positive for anti-cyclic citrullinated peptide antibodies, but their sera also react with unmodified arginine-containing peptide. Arthritis Rheum. *58*, 1576–1581. https://doi.org/10.1002/art.23514.
125. Balbi, G.G.M., Machado-Ribeiro, F., Marques, C.D., Signorelli, F., and Levy, R.A. (2018). The interplay between tuberculosis and systemic lupus erythematosus. Curr. Opin. Rheumatol. *30*, 395–402. https://doi.org/10.1097/BOR.0000000000000493.
126. Dutta, N.K., and Karakousis, P.C. (2014). Latent tuberculosis infection: myths, models, and molecular mechanisms. Microbiol. Mol. Biol. Rev. *78*, 343–371. https://doi.org/10.1128/MMBR.00010-14.
127. Fennelly, K.P., and Jones-Lopez, E.C. (2015). Quantity and Quality of Inhaled Dose Predicts Immunopathology in Tuberculosis. Front. Immunol. *6*, 313. https://doi.org/10.3389/fimmu.2015.00313.
128. Zhang, Y., and Wang, H. (2012). Integrin signalling and function in immune cells. Immunology *135*, 268–275. https://doi.org/10.1111/j.1365-2567.2011.03549.x.
129. Yusuf-Makagiansar, H., Anderson, M.E., Yakovleva, T.V., Murray, J.S., and Siahaan, T.J. (2002). Inhibition of LFA-1/ICAM-1 and VLA-4/VCAM-1 as a therapeutic approach to inflammation and autoimmune diseases. Med. Res. Rev. *22*, 146–167. https://doi.org/10.1002/med.10001.
130. Luo, B.H., Carman, C.V., and Springer, T.A. (2007). Structural basis of integrin regulation and signaling. Annu. Rev. Immunol. *25*, 619–647. https://doi.org/10.1146/annurev.immunol.25.022106.141618.
131. Martin, F., and Kearney, J.F. (2002). Marginal-zone B cells. Nat. Rev. Immunol. *2*, 323–335. https://doi.org/10.1038/nri799.
132. Amsen, D., Blander, J., Lee, G.R., Tanigaki, K., Honjo, T., and Flavell, R.A. (2004). Instruction of distinct CD4 T helper cell fates by different notch ligands on antigen-presenting cells. Cell *117*, 515–526. https://doi.org/10.1016/s0092-8674(04)00451-9.
133. Maekawa, Y., Minato, Y., Ishifune, C., Kurihara, T., Kitamura, A., Kojima, H., Yagita, H., Sakata-Yanagimoto, M., Saito, T., Taniuchi, I., et al. (2008). Notch2 integrates signaling by the transcription factors RBP-J and CREB1 to promote T cell cytotoxicity. Nat. Immunol. *9*, 1140–1147. https://doi.org/10.1038/ni.1649.
134. Lewis, K.L., Caton, M.L., Bogunovic, M., Greter, M., Grajkowska, L.T., Ng, D., Klinakis, A., Charo, I.F., Jung, S., Gommerman, J.L., et al. (2011). Notch2 receptor signaling controls functional differentiation of dendritic cells in the spleen and intestine. Immunity *35*, 780–791. https://doi.org/10.1016/j.immuni.2011.08.013.
135. Sakata-Yanagimoto, M., Sakai, T., Miyake, Y., Saito, T.I., Maruyama, H., Morishita, Y., Nakagami-Yamaguchi, E., Kumano, K., Yagita, H., Fukayama, M., et al. (2011). Notch2 signaling is required for proper mast cell distribution and mucosal immunity in the intestine. Blood *117*, 128–134. https://doi.org/10.1182/blood-2010-07-289611.
136. Picelli, S., Faridani, O.R., Björklund, Å.K., Winberg, G., Sagasser, S., and Sandberg, R. (2014). Full-length RNA-seq from single cells using Smart-seq2. Nat. Protoc. *9*, 171–181. https://doi.org/10.1038/nprot.2014.006.
137. Dobin, A., Davis, C.A., Schlesinger, F., Drenkow, J., Zaleski, C., Jha, S., Batut, P., Chaisson, M., and Gingeras, T.R. (2013). STAR: ultrafast universal RNA-seq aligner. Bioinformatics *29*, 15–21. https://doi.org/10.1093/bioinformatics/bts635.
138. Cunningham, F., Allen, J.E., Allen, J., Alvarez-Jarreta, J., Amode, M.R., Armean, I.M., Austine-Orimoloye, O., Azov, A.G., Barnes, I., Bennett, R., et al. (2022). Ensembl 2022. Nucleic Acids Res. *50*, D988–D995. https://doi.org/10.1093/nar/gkab1049.
139. Love, M.I., Huber, W., and Anders, S. (2014). Moderated estimation of fold change and dispersion for RNA-seq data with DESeq2. Genome Biol. *15*, 550. https://doi.org/10.1186/s13059-014-0550-8.
140. Kolde, R. (2019). pheatmap: Pretty Heatmaps. R package version 1.0. 12.

STAR★METHODS

KEY RESOURCES TABLE

REAGENT or RESOURCE	SOURCE	IDENTIFIER
Antibodies		
CD45- Alexa Fluor700 (30-F11)	Biolegend	Cat#103128; RRID:AB_493715
B220-BUV395 (RA3-6B2)	BD Bioscience	Cat#563793; RRID:AB_2738427
CD93-PE-Cy7 (AA4.1)	Biolegend	Cat#136504; RRID:AB_1967094
CD21/35-FITC (7E9)	Biolegend	Cat#123408; RRID:AB_940403
CD23-PE (B3B4)	Biolegend	Cat#101608; RRID:AB_312833
CD1d-BV421 (1B1)	BD Bioscience	Cat#562712; RRID:AB_2737739
CD86-APC (GL-1)	Biolegend	Cat#105012; RRID:AB_493342
CD69-BV605 (H1.2F3)	Biolegend	Cat#104530; RRID:AB_2563062
CD43-BV510 (S7)	BD Bioscience	Cat#563206; RRID:AB_2738069
CD43-BV480 (S7)	BD Bioscience	Cat#746633; RRID:AB_2743912
CD3-APC-eFluor 780 (17A2)	Thermo Fisher Scientific	Cat#47-0032-82; RRID:AB_1272181
CD335-APC-eFluor 780 (29A1.4)	Thermo Fisher Scientific	Cat#47-3351-82; RRID:AB_2573980
B220-BUV496 (RA3-6B2)	BD Bioscience	Cat#612950; RRID:AB_2870227
CD19-BV785 (6D5)	Biolegend	Cat#115543; RRID:AB_11218994
CD23-PE-Cy7 (B3B4)	Biolegend	Cat#101614; RRID:AB_2103037
IgM-FITC (RMM-1)	Biolegend	Cat#406506; RRID:AB_315055
IgD-BUV395 (11-26c.2a)	BD Bioscience	Cat#564274; RRID:AB_2738723
CD69-PE (H1.2F3)	Biolegend	Cat#104508; RRID:AB_313110
CD5-BUV737 (53-7.3)	BD Bioscience	Cat#612809; RRID:AB_2870134
CD138-BV605 (281-2)	Biolegend	Cat#142516; RRID:AB_2562337
B220-FITC (RA3-6B2)	Biolegend	Cat# 103206; RRID: AB_312991
CD80-BV605 (15-10A1)	Biolegend	Cat#104729; RRID: AB_11126141
PD-L2-BUV395 (TY25)	BD Bioscience	Cat#565102; RRID: AB_2739068
CD73-APC (TY/11.8)	Biolegend	Cat#127210; RRID: AB_11218786

(*Continued on next page*)

Continued

REAGENT or RESOURCE	SOURCE	IDENTIFIER
CD3-BV605 (17-A2)	Biolegend	Cat#100237; RRID:AB_2562039
CD4-BUV395 (GK1.5)	BD Bioscience	Cat#565974; RRID:AB_2739427
CD8a-PerCP-eFlour710 (53-6.7)	Thermo Fisher Scientific	Cat#46-0081-82; RRID:AB_1834433
CD103-BV421 (2E7)	Biolegend	Cat#121422; RRID:AB_10900074
γδTCR-FITC (GL3)	Biolegend	Cat#118106; RRID:AB_313829
CD335-PE-Cy7 (29A1.4)	Biolegend	Cat#137618; RRID:AB_11218594
PD-1-BV785 (29F.1A12)	Biolegend	Cat#135225; RRID:AB_2563680
CD1d tetramer-APC (PSB-57)	NIH Tetramer core facility	N/A
Fc Block (2.4G2)	BD Bioscience	Cat#553141; RRID:AB_394656
CXCL1- Alexa Fluor647 (1174A)	R&D SYSTEMS	Cat#IC4532R
CCL5-PE (2E9)	Biolegend	Cat#149104; RRID:AB_2564405
GM-CSF-PE (MP1-22E9)	BD Bioscience	Cat#554406; RRID:AB_395371
IL-2-BV605 (JES6-5H4)	BD Bioscience	Cat# 563911; RRID:AB_2738482
TNF-α-APC (MP6-XT22)	Biolegend	Cat#506308; RRID:AB_315429
CD11a antibody (M17/4)	Thermo Fisher Scientific	Cat# 16-0111-85; RRID:AB_468882
CD49d antibody (R1-2)	Thermo Fisher Scientific	Cat# 16-0492-85; RRID:AB_468970
Rat isotype IgG2a (eBR2a)	Thermo Fisher Scientific	Cat# 16-4321-85; RRID:AB_470157
Rat isotype IgG2b (eB149/10H5)	Thermo Fisher Scientific	Cat# 16-4031-85; RRID:AB_470152
Goat Anti-Mouse IgM-HRP	Southern Biotech	Cat# 1020-05; RRID:AB_2794201
Goat Anti-Mouse IgG-HRP	Southern Biotech	Cat# 1030-05; RRID:AB_2619742
Goat Anti-Mouse IgA-HRP	Southern Biotech	Cat# 1040-05; RRID:AB_2714213
B220- Alexa Fluor488 (RA3-6B2)	BD Bioscience	Cat# 557669; RRID:AB_396781
CD1d- Alexa Fluor647 (1B1)	BD Bioscience	Cat# 564706; RRID:AB_2738905
Rat isotype IgG2b (A95-1)	BD Bioscience	Cat# 557691; RRID:AB_396800
Bacterial and virus strains		
Mycobacterium tuberculosis H37Rv	ATCC	Cat#27294
Biological samples		
Mycobacterium tuberculosis, H37Rv, Gamma-Irradiated Whole Cells	bei RESOURCES	Cat#NR-49098

(*Continued on next page*)

Continued

REAGENT or RESOURCE	SOURCE	IDENTIFIER
Mycobacterium tuberculosis, H37Rv, Whole Cell Lysate	bei RESOURCES	Cat#NR-14822
Tuberculin purified protein derivative (PPD)	Statens Serum Institut	N/A
Chemicals, peptides, and recombinant proteins		
Horizon Brilliant Stain Buffer	BD Bioscience	Cat#563794
Horizon Brilliant Stain Buffer Plus	BD Bioscience	Cat#566385
GolgiStop	BD Bioscience	Cat#554724
GolgiPlug	BD Bioscience	Cat#555029
Cytofix/Cytoperm solution	BD Bioscience	Cat#554722; AB_2869010
Perm/Wash buffer	BD Bioscience	Cat#554723
ACK lysing buffer	Thermo Fisher Scientific	Cat#A1049201
LIVE/DEAD Fixable Near-IR Dead Cell Stain Kit, for 633 or 635 nm excitation	Thermo Fisher Scientific	Cat#L34976
Liberase TL	Sigma-Aldrich	Cat#5401020001
CountBright	Thermo Fisher Scientific	Cat#C36950
RPMI-1640	Cytiva HyClone	Cat#SH30027.FS
Fetal calf serum	Cytiva HyClone	Cat#SH30088.03
Sodium pyruvate	Thermo Fisher Scientific	Cat#11360070
HEPES	Thermo Fisher Scientific	Cat#15630080
L-Glutamine	Thermo Fisher Scientific	Cat#25030081
TRIzol	Thermo Fisher Scientific	Cat#15596026
Bovine Serum Albumin (BSA)	Sigma-Aldrich	Cat#A7906
ELISA Coating Buffer	Biolegend	Cat#421701
TMB substrate set	Biolegend	Cat#421101
Middlebrook 7H11 agar	BD	Cat#283810
OADC Enrichment	BD	Cat#212351
DAPI (4',6-Diamidino-2-Phenylindole, Dihydrochloride)	Thermo Fisher Scientific	Cat#D1306
ProLong™ Diamond Antifade Mountant	Thermo Fisher Scientific	Cat#P36965
O.C.T. Compound	Fisher Scientific	Cat#FIS23-730-571
Critical commercial assays		
Bio-Plex Pro Mouse Cytokine 23-plex Assay	BIO-RAD	Cat#M60009RDPD; AB_2857368
RNeasy Micro kit	Qiagen	Cat#74004
DNA High Sensitivity Reagent Kit	PerkinElmer	Cat#CLS760672
Deposited data		
RNA seq of B cells from Mtb-infected and control mice	This study	SRA data: PRJNA1034093
Experimental models: Organisms/strains		
Mouse: BALB/cJInv	InVivos	N/A
Mouse: BALB/cAnNCrl	Charles River	N/A
Oligonucleotides		
Template Switching Oligo (5′-AAGCAGT GGTATCAACGCAGAGTACATrGrG+G-3′)	S Picelli et al., 2014	N/A
Software and algorithms		
Flowjo Version10.8.2	BD Bioscience	RRID:SCR_008520 https://www.flowjo.com/solutions/flowjo/downloads

(*Continued on next page*)

Continued

REAGENT or RESOURCE	SOURCE	IDENTIFIER
Prism 9	GraphPad	RRID:SCR_002798 http://www.graphpad.com/
STAR version 2.7.1b	Dobin A et al., 2013[137]	RRID:SCR_004463 https://github.com/alexdobin/STAR/releases
R package DESeq2	MI Love et al., 2014[139]	RRID:SCR_015687 https://bioconductor.org/packages/release/bioc/html/DESeq2.html
Pretty Heatmaps. R package version 1.0.12	R Kolde et al., 2019[140]	RRID:SCR_016418 https://cran.r-project.org/web/packages/pheatmap/index.html
Belysa software version 1.2.1	Millipore Sigma	https://www.sigmaaldrich.com/US/en/services/software-and-digital-platforms/belysa-immunoassay-curve-fitting-software
LAS X Life Science Microscope Software Platform 4.6.1	Leica Microsystems	RRID:SCR_01367 https://www.leica-microsystems.com/products/microscope-software/p/leica-las-x-ls/
Other		
C Tubes	Miltenyi Biotec	Cat#130-093-237
U-shaped-bottom 96-well plate	Corning	Cat#3799
96-well flat-bottom plates (MaxiSorp, Nunc)	Thermo Fisher Scientific	Cat#442404
Micro Cover Glasses, Square, No. 11/2	VWR	Cat#48366-227

RESOURCE AVAILABILITY

Lead contact

Further information and requests for resources and reagents should be directed to and will be fulfilled by the lead contact, Martin Gengenbacher (martin.gengenbacher@gmail.com)

Materials availability

The study did not generate new unique reagents

Data and code availability

- The RNA-seq data of B cells from this study are deposited in the NCBI BioProject database under the accession number PRJNA1034093.
- This paper does not report original code.
- Any additional information required to reanalyze the data reported in this paper is available from the lead contact upon request.

EXPERIMENTAL MODEL AND SUBJECT DETAILS

Mice and aerosol infection

Six- to ten-week-old, female, specific pathogen-free BALB/c mice were obtained from InVivos, Singapore and Charles River, USA. Mice were housed in the Animal Biosafety Level 3 laboratory (ABSL-3) at National University of Singapore and Center for Discovery and Innovation, Hackensack Meridian Health. Mice were provided *ad libitum* access to water and food, housed in groups of 2-5 mice per cage, and maintained under controlled temperature, humidity, and light cycle. For aerosol infection, each mouse was infected with 100-200 colony-forming unit (CFU) of aerosolized Mtb H37Rv (ATCC#27294) using a Full Body Inhalation Exposure System (Glascol). Mice in the mock-infected control groups were exposed to the same amount of aerosolized gamma-irradiated Mtb H37Rv (BEI Resources, NR-49098) using the same system. Uninfected mice served as uninfected controls. Mice were euthanized at designated time points post-infection for analysis. The use of experimental animals has been approved by the Institutional Animal Care and Use Committee, National University of Singapore (Protocol R14-0911) and Center for Discovery and Innovation, Hackensack Meridian Health (Protocol 265).

Enumeration of tissue bacterial load

The lungs and spleen were harvested from infected mice and homogenized in 1ml of phosphate-buffered saline containing 0.05% Tween 80 (PBST). Organ homogenates were serially diluted 10-fold in PBST, and 100μl of each serial dilution was plated onto Middlebrook 7H11 agar (BD Difco) supplemented with 0.5% glycerol and 10% oleic acid-albumin-dextrose-catalase enrichment (OADC). Bacterial loads were measured by counting the colonies on plates after incubation for 3-4 weeks at 37°C.

Preparation of single-cell suspensions

Single-cell suspensions of the lungs and spleen were prepared using gentleMACS C Tubes (Miltenyi Biotec) and the gentleMACS Dissociator (Miltenyi Biotec). For the lungs, lung lobes were placed into C-tubes containing 2.5 ml of RPMI-1640 (Hyclone) with 50μg/ml of Liberase TL (Sigma-Aldrich) and dissociated using the program "m_lung_01". Subsequently, the lungs were digested at 37°C for 1 hour and further dissociated using the program "m_lung_02". For the spleen, the spleen was placed into C-tubes containing 2.5 ml of RPMI-1640 (Hyclone) and directly dissociated using the program "m_spleen_02".

Subsequently, the resulting cell suspensions were filtered through 70 μm cell strainers (Miltenyi Biotec) and washed with 10ml of MACS buffer (PBS containing 0.5% BSA and 2 mM EDTA) by centrifuging at 500x g for 5 minutes at 4°C and removing supernatants. The cell suspensions were treated with 1ml of ACK lysing buffer (Thermo Fisher Scientific) for 5 minutes to remove red blood cells and washed with MACS buffer again as described above. Finally, the cells were resuspended in 2ml of MACS buffer for further analysis.

Flow cytometry

Cell numbers of the single-cell suspensions were determined using an automated cell counter (LUNA-II, Logos Biosystems). The cells were normalized and seeded at 1-2 x 10^6 cells/well in U-shaped-bottom 96-well plates (Corning). The cells were centrifuged at 500x g for 5 minutes at 4°C, MACS buffer was removed, and subsequently the cells were washed with 200μl of PBS. After centrifuging again, PBS was removed. To distinguish live and dead cells, the cells were stained with LIVE/DEAD Fixable Near-IR Dead Cell Stain Kit (Thermo Fisher Scientific) at 1:1000 dilution in 200μl of PBS for 20 minutes at 4°C and washed again with PBS. To block Fc gamma receptors, the cells were incubated with Fc Block (BD Biosciences) at 5μg/ml in 40μl of FACS buffer (PBS containing 1% BSA, 0.05% sodium azide) for 5-10 minutes at room temperature. Subsequently, to stain the cells, 60μl of the antibody cocktails were added and incubated for 20 minutes at room temperature. Excess antibodies were removed by washing with 200μl of FACS buffer twice and aspirating the supernatant completely. Finally, to fix and permeabilize the cells, cells were resuspended and incubated with 200μl of Cytofix/Cytoperm buffer (BD Biosciences) for 1 hour at room temperature. Fixed cells were transferred to clean round-bottom 96-well plates (Corning) and shipped out from the BSL-3 laboratories. To remove the excess Cytofix/Cytoperm solution (BD Biosciences), the cells were washed with 200μl of FACS buffer twice, resuspended, and stored in 200μl of FACS buffer at 4°C for flow cytometric analysis or intracellular staining.

For intracellular staining, cells were centrifuged to remove FACS buffer and permeabilized in 50μl of Perm/Wash buffer (BD Biosciences) with Fc Block (5μg/ml, BD Biosciences) for 30 minutes at room temperature. Subsequently, 50μl of antibody cocktails were added and incubated for 20 minutes at room temperature. The excessive antibodies were removed by washing twice with 200μl of Perm/Wash buffer (BD Biosciences), and the cells were stored in 200μl of FACS buffer at 4°C for flow cytometric analysis.

Before flow cytometric analysis, cells were resuspended in 380μl of FACS buffer, and 20μl of absolute counting beads were added to enable the analysis of absolute counts (CountBright, Thermo Fisher Scientific). Data were acquired using the LSR Fortessa X-20 flow cytometer (BD Biosciences) or BD FACSymphony A3 (BD Biosciences) and analyzed by FlowJo software v10 (BD Biosciences).

Antibodies and reagents for flow cytometry analysis

Four major staining panels were used in this study. The panel 1: CD45- Alexa Fluor700 (30-F11), B220-BUV395 (RA3-6B2), CD93-PE.Cy7 (AA4.1), CD21/35-FITC (7E9), CD23-PE (B3B4), CD1d-BV421 (1B1), CD86-APC (GL-1), CD69-BV605 (H1.2F3), CD43-BV510 or CD43-BV480 (S7) and the dump channel: CD3-APC-eFluor 780 (17A2) and CD335-APC-eFluor 780 (Clone: 29A1.4). The panel 2: CD45- Alexa Fluor 700 (Clone: 30-F11), B220-BUV496 (RA3-6B2), CD19-BV785 (6D5), CD23-PE.Cy7 (B3B4), CD1d-BV421 (1B1), IgM-FITC (RMM-1), IgD-BUV395 (11-26c.2a), CD86-APC (GL-1), CD69-PE (H1.2F3), CD5-BUV737 (53-7.3), CD138-BV605 (281-2), CD43-BV510 or CD43-BV480 (S7), the dump channel: CD3-APC-eFluor 780 (17A2) and CD335-APC-eFluor 780 (29A1.4). The panel 3: CD45- Alexa Fluor700 (30-F11), CD3-BV605 (17-A2), CD4-BUV395 (GK1.5), CD8a-PerCP-eFlour710 (53-6.7), CD69-PE (H1.2F3), CD103-BV421 (2E7), γδTCR-FITC (GL3), CD335-PE.Cy7 (29A1.4), B220-BUV496 (RA3-6B2), PD-1-BV785 (29F.1A12), CD1d tetramer-APC (PSB-57). The panel 4: CD45- Alexa Fluor700 (30-F11), B220-FITC (RA3-6B2), CD93-PE.Cy7 (AA4.1), CD23-PE (B3B4), CD1d-BV421 (1B1), CD80-BV605 (15-10A1), PD-L2-BUV395 (TY25), CD73-APC (TY/11.8), and the dump channel: CD3-APC-eFluor 780 (17A2) and CD335-APC-eFluor 780 (29A1.4). To make the antibody cocktails for staining, antibodies in each panel were mixed in staining buffer (Brilliant Stain Buffer) in 60μl total volume. All panels included LIVE/DEAD staining (Fixable Near-IR Dead Cell Stain Kit) to distinguish dead cells. All cells were treated by Fc block (2.4G2) before staining. For intracellular staining, CXCL1- Alexa Fluor647 (1174A) and CCL5-PE (2E9), GM-CSF-PE (MP1-22E9), and IL-2-BV605 (JES6-5H4), and TNF-α-APC (MP6-XT22) were used for detecting cytokine production. The antibody cocktails for intracellular staining were mixed with 10μl of the staining buffer (Horizon Brilliant Stain Buffer Plus) and Perm/Wash Buffer into 50μl total volume.

Ex vivo restimulation of cells

The experiments were conducted in the Biosafety Level 3 laboratory (BSL-3) at Center for Discovery and Innovation, Hackensack Meridian Health. Single-cell suspensions of lungs and spleen were prepared as described above but washed and resuspended in RPMI-2 (PMI-1640, 2% fetal calf serum, 1mM sodium pyruvate, 20mM HEPES, 1mM L-Glutamine) for the final step and stored at 4°C overnight. Subsequently, the cells were seeded into 2 x 10^6 cells in 200ul of RPMI-2 per well in U-shaped-bottom 96-well plates (Corning) and incubated in the cell incubator for 30 minutes at 37°C, 5% CO_2. The cells were re-stimulated by Mtb lysate (40μg/ml, H37Rv, BEI Resources) and incubated with GolgiStop (1:1500 dilution) and GolgiPlug (1:1000 dilution) in the cell incubator for 5.5 hours at 37°C, 5% CO_2. At the end of the experiments, cells were stained with surface markers and intracellular cytokines, as described above.

Cell sorting

Mice (six- to eight-week-old, BALB/c, female, InVivos) were infected with aerosolized Mtb (H37Rv, 100-200 CFU per mouse) as described above. Uninfected mice served as uninfected controls. Single-cell suspensions of the lungs and spleen were generated as described above. Subsequently, single-cell suspensions from 12 mice were pooled and stained for the surface markers. The staining procedure was similar to that described above, but the cells were stained in 15ml tubes (Falcon). FACS buffer used for staining and washing contained no sodium azide. Live and dead cells were distinguished by LIVE/DEAD staining. The staining panel used to distinguish MZB and FoB cells included: CD45- Alexa Fluor700 (30-F11), B220-BUV395 (RA3-6B2), CD93-PE.Cy7 (AA4.1), CD21/35-FITC (7E9), CD23-PE (B3B4), CD1d-BV421 (1B1), CD86-APC (GL-1) and the dump channel: CD3-APC-eFluor 780 (17A2) and CD335-APC-eFluor 780 (Clone: 29A1.4). After staining, the cells were resuspended in MACS buffer at 2 x 10^6 cells/100ul for cell sorting. MZB and FoB cells were purified using a cell sorter (FACSAria Fusion, BD) under BSL-3 conditions. MZB and FoB cells were respectively sorted into 15ml tubes containing FACS buffer. After cell sorting, the cells were centrifuged at 500x g for 15 minutes at 4°C, and the FACS buffer was completely removed. Finally, the cells were resuspended in 2ml of Trizol (Thermo Fisher Scientific) and stored at -20°C.

Depletion of MZB cells

To deplete MZB cells, mice (six- to eight-week-old, BALB/c, female, InVivos) were injected intraperitoneally with 100μg of anti-CD11a antibody (M17/4) and 100μg of anti-CD49d antibody (R1-2) one day before infection[60–63]. The control mice were injected intraperitoneally with 100μg of rat isotype IgG2a (eBR2a, eBioscience) and 100μg of rat isotype IgG2b (eB149/10H5, eBioscience). Subsequently, mice were infected with aerosolized Mtb (H37Rv,100-200 CFU per mouse), as described above. Infected mice in the experimental group continuously received the same amount of depletion antibodies every week until sacrifice. Similarly, infected mice in the control group continuously received the same amount of relevant isotype control antibodies every week as the depletion protocol. Mice were euthanized at 2-, 4-, 6-, and 8-weeks post-infection.

Antimycobacterial chemotherapy

Mice (six- to eight-week-old, BALB/c, female, InVivos) were infected with aerosolized Mtb (H37Rv, 100-200 CFU per mouse) and kept for 8 weeks to develop immunophenotypic changes of B cells. At 8 weeks post-infection, Infected mice in the experimental group received an antibiotic regime in drinking water containing 100 mg/L isoniazid (Sigma-Aldrich) and 100 mg/L rifabutin (Sigma-Aldrich). Infected mice in the control group received regular drinking water. Uninfected mice that received the same antibiotic regimen served as uninfected controls. Mice were sacrificed at 2 and 6 weeks after initiating treatment. To avoid carry-over antibiotics affecting CFU determination, treated mice were shifted back to regular drinking water 3 days before sacrifice. In addition, 7H11 agar plates containing 10% OADC and activated charcoal were used for CFU quantification.

Plasma sample collection

Whole blood was collected from hearts into heparinized tubes (BD) and mixed by gently inverting the tubes. Subsequently, the tubes were centrifuged at 300x g for 10 minutes at 4°C. The resulting supernatants were the plasma samples. The plasma samples were filtered twice using 0.22 μm tube filters (Spin X, Corning, Costar) and stored at -20°C.

ELISA

The levels of PPD-reactive IgM, IgG, and IgA in plasma samples were measured by PPD ELISA, according to the previous publication[33]. For the preparation of the ELISA plates, 96-well flat-bottom plates (MaxiSorp, Nunc, Thermo Fisher Scientific) were coated with 100μl of PDD (5μg/ml, Statens Serum Institut) in coating buffer (PH 9.5, Biolegend) per well for 2 hours at room temperature. Subsequently, each well was washed with 200μl of wash buffer (PBS with 0.05% Tween 20) three times and added 300μl of blocking buffer (PBS with 2% BSA, 0.05% Tween 20) for overnight incubation at 4°C. The blocking buffer was removed before adding samples.

Plasma samples underwent serial dilution in diluted buffer (PBS with 2% BSA, 0.05% Tween 20), beginning at a 1:10 dilution and proceeding to 1:50, 1:250, and 1:1250. Subsequently, 50μl of diluted sample was added into each well and incubated for 1 hour at room temperature. The plates were washed three times with washing buffer and further incubated with 50μl of diluted horseradish peroxidase (HRP)-conjugated detection antibodies in each well for 1 hour at room temperature. Goat Anti-Mouse IgM-HRP was used for detecting PPD-reactive IgM (1:4000 in diluted buffer, Cat. No.1020-05, Southern Biotech); Goat Anti-Mouse IgG-HRP was

used for detecting PPD-reactive IgG (1:4000 in diluted buffer, Cat. No. 1030-05, Southern Biotech); Goat Anti-Mouse IgA-HRP was used for detecting PPD-reactive IgA (1:4000 in diluted buffer, Cat. No. 1040-05, Southern Biotech).

After washing the plates three times with the wash buffer, 100μl of TMB substrate (Biolegend) was added to each well and incubated at room temperature until the optimal color intensity was reached. The incubation time for PPD-reactive IgM detection was 14 minutes, and for both PPD-reactive IgG and IgA was 30 minutes. Finally, 50μl of stop solution (Biolegend) was added to each well to terminate the reaction. The plates were read using a microplate reader (Tecan M200 Infinite Pro). Absorbance at 450nm was measured and corrected with absorbance at 570 nm. Dilutions within linear ranges of optical density at 450nm (OD450) were selected for analysis. For PPD-reactive IgM, a 1:50 dilution was used, corresponding to an OD450 range from 0 to 2. For PPD-reactive IgG, a 1:250 dilution was selected, corresponding to an OD450 range from 0 to 1.6. Due to low levels of PPD-reactive IgA, the most concentrated dilution of 1:10 was selected.

Multiplex analysis of cytokines

The levels of cytokines in plasma samples were detected using the Bio-Plex Pro Mouse Cytokine 23-plex Assay (Bio-Rad) according to the manufacturer's protocol. Briefly, 50μl of coupled beads was added into each well of 96-well, flat-bottom plates, and the plates were washed on magnetic separators. The plates were washed twice with 100μl of Bio-Plex wash buffer per well. The plasma samples were diluted 1:4 in Bio-Plex sample diluent. Subsequently, 50μl of diluted samples, standards, and blanks (sample diluent) was added to the designated wells and incubated at room temperature for 1 hour with shaking (850 rpm). After incubation, plates were washed three times with 100μl of Bio-Plex wash buffer per well on a magnetic separator. 25μl of detection antibodies (1x) was added into each well and incubated at room temperature for 30 minutes with shaking (850 rmp). Plates were washed three times using the same procedures. 50μl of Streptavidin-PE (1x) was added into each well and incubated at room temperature for 10 minutes with shaking (850 rmp). After incubation, plates were washed three times, following the same procedures, and the beads in each well were resuspended in 125μl of assay buffer. The beads on plates were analyzed on a MAGPIX following the manufacturer's manual. The raw data were analyzed using Belysa software (version 1.2.1, Millipore Sigma).

Library preparation and RNA-Seq processing

Sorted B cells were frozen in TRIzol (Thermo Fisher Scientific). Total RNA was extracted using acid guanidinium thiocyanate-phenol-chloroform extraction and subsequently cleaned up using RNeasy Micro kit (Qiagen). The RNA quality was assessed on the Bioanalyzer (Agilent) with RNA Integrity Number (RIN) ranging from 7.4 to 9.9. cDNA libraries were prepared using 2 ng of total RNA following the Smart-seq2 protocol[136] with specific modifications: (1) the addition of 20 μM Template Switching Oligo (TSO), and (2) the use of 200 pg of cDNA with one-fifth of a reaction from the Illumina Nextera XT Kit (Illumina). The length distribution of the cDNA libraries was determined using a DNA High Sensitivity Reagent Kit on the Labchip system (PerkinElmer). All samples were subjected to an indexed paired-end sequencing run of 2 x 151 cycles using the HiSeq 4000 system (Illumina), with 24 samples allocated per lane.

Reads mapping and quantification

Raw sequencing reads were processed and aligned using the standard protocol and parameters from STAR version 2.7.1b to obtain gene counts[137]. Reads were aligned to the Ensemble Mus musculus genome and annotations version GRCm39.106[138]. Gene counts were further analyzed for differential expression using R package DESeq2[139], and contrasts were made between cell types (MZB vs. FoB). The 30 genes with the most significant normalized expression levels were identified and ranked by the lowest adjusted *p*-value for this contrast. These expression levels were normalized using DESeq2 median of ratios. The adjusted *p*-value was corrected using the Benjamini-Hochberg method at a False Discovery Rate (FDR) < 0.05. Expression levels were visualized using the R package pheatmap[140].

Immunostaining and confocal microscopy

Lungs and spleen were harvested following perfusion with 1ml of PBS and stored at -80°C. To inactivate Mtb, the samples were γ-irradiated prior to cryosection (National Institutes of Health, USA). Each sample was embedded in O.C.T. compound (Fisher Scientific) and sectioned at a thickness of 10μm using a cryostat (CM1860 UV, Leica Biosystems). Sections were air-dried for 1 hour at room temperature and fixed with 4% paraformaldehyde (Image-iT™ Fixative Solutions, Thermo Scientific) for 8 minutes. After fixation, sections were washed three times with PBS for 10 minutes each and blocked with blocking buffer (PBS with 1% BSA) for 30 minutes. Sections were stained with B220-Alexa Fluor 488 (RA3-6B2) and CD1d-Alexa Fluor 488 (1B1) at a 1:100 dilution for 1 hour at room temperature, followed by three PBS washes. Sections were further stained with 4',6-Diamidino-2-Phenylindole, Dihydrochloride (DAPI, Thermo Scientific) at a 1:1000 dilution for 5 minutes, then washed three times with PBS. Finally, sections were mounted with mounting media (ProLong™ Diamond Antifade Mountant, Thermo Scientific) and covered with coverslips (Micro Cover Glasses, Square, No. 11/2, VWR). Imaging was performed on a Leica Stellaris 5 confocal microscope (Leica Microsystems) and processed using LAS X Life Science Microscope Software Platform (Leica Microsystems).

QUANTIFICATION AND STATISTICAL ANALYSIS

Flow cytometry data were analyzed by FlowJo software v10 (BD Biosciences). The gating strategies are depicted in Figures S1A, S2I, S3, S5A, S6C, and S6D. Fluorescence Minus One (FMO) controls were used to identify cells expressing CD9, CD43, CD69, CD73, CD80, CD86, TACI, CD138, CD273, cytokine and chemokines. Representative flow cytometry data are shown as contour plots, histograms, or dot plots. Contour plots are displayed with 5% contour levels and outliers; histograms are illustrated using the modal option, where the Y-axis represents the frequency of maximum cell counts; Dot plots display a maximum of 8,000 events. Statistical analyses and data visualization were performed using Prism software v9 (GraphPad). Scatter plots feature horizontal lines representing the mean. Line and bar charts depict data as mean ± standard error of the mean (SEM). Error bars are omitted when shorter than the height of the symbols. The n number represents biological replicates for mice. Unpaired or paired two-tailed Student's t-test was used to determine the statistical differences between the two groups. One-way ANOVA or One-way repeated measures ANOVA with Bonferroni's post hoc test was used to determine the statistical differences among three or more groups. A p-value <0.05 was considered significant (*p <0.05 **p <0.01 ***p<0.001, ****p<0.0001. ns, not significant). Normality was examined using Shapiro-Wilk test, Anderson-Darling test, Kolmogorov-Smirnov test and quantile-quantile plots. For RNA-Seq data, gene counts were analyzed for differential expression using R package DESeq2[139], and contrasts were made between cell types. The significant normalized expression levels were ranked by the adjusted p-value for each contrast. These expression levels were normalized using the DESeq2 median of ratios. The adjusted p-value was corrected using the Benjamini-Hochberg method at a False Discovery Rate (FDR) < 0.05. The details about sample sizes, statistical tests, and replication frequencies are indicated within individual figure legends.